DOI: 10.1002/chem.200600693

Reaction Chemistry of Complexes Containing Pt–H, Pt–SH, or Pt–S Fragments: From Their Apparent Simplicity to the Maze of Reactions Underlying Their Interconversion

Fernando Novio, Pilar González-Duarte,* Agustí Lledós,* and Rubén Mas-Ballesté[a]

Abstract: The relevance of platinum in the reaction of thiophene and derivatives with homogeneous transition-metal complexes as models for hydrodesulfurization has led us to the study of the reaction chemistry of complexes containing Pt–H, Pt–SH, and Pt–S fragments. Exploration of the reactions triggered by addition of controlled amounts of Na_2S or NaSH to $[Pt_2(H)_2(\mu\text{-}H)(dppp)_2]ClO_4$ (**1**) has provided evidence of the formation of complexes $[Pt_2(\mu\text{-}H)(\mu\text{-}S)(dppp)_2]ClO_4$ (**2**), $[Pt(H)(SH)(dppp)]$ (**3**), $[Pt_2(\mu\text{-}S)_2(dppp)_2]$ (**4**), $[Pt_2(\mu\text{-}S)(dppp)_2]$ (**5**) and $[Pt(SH)_2(dppp)]$, in which dppp denotes 1,3-bis(diphenylphosphanyl)propane. Consequently, complexes **1**, **2**, and **5** as well as the already reported **3**, **4**, and $[Pt(SH)_2(dppp)]$ have been obtained and fully characterized spectroscopically. Also the crystal structures of **1** and **2** have been solved. Complexes **1**–**5** constitute the main framework of the network of reactions that account for the evolution of **1** under various experimental conditions as shown in Scheme 1. Apparently, this network has complexes **2** and **4** as dead-ends. However, their reciprocal interconversion by means of the replacement of one bridging hydride or sulfide ligand in the respective $\{Pt(\mu\text{-}H)(\mu\text{-}S)Pt\}$ and $\{Pt(\mu\text{-}S)_2Pt\}$ cores enables the closure of the reaction cycle involving complexes **1**–**5**. Theoretical calculations support the existence of the undetected intermediates proposed for conversion from **1** to **2** and from **3** to **2** and also account for the fluxional behavior of **1** in solution. The intermediates proposed are consistent with the experimental results obtained in comparable reactions carried out with labeled reagents, which have provided evidence that complex **1** is the source of the hydride ligands in complexes **2** and **3**. Overall, our results show the strong dependence on the experimental conditions for the formation of complexes **1**–**5** as well as for their further conversion in solution.

Keywords: hydride ligands · phosphane ligands · platinum · S ligands · structure elucidation

Introduction

The removal of sulfur from petroleum feedstock is one of the most extensively investigated industrial processes.[1] Over the past decade, interest in this process has been fueled by new legislation directed at reducing the current sulfur levels of 300–500 ppm in gasoline and diesel,[2] and also by the need to avoid poisoning of the precious metal-based catalysts that are used in producing high octane gasoline. Hydrodesulfurization (HDS) is the commonly used commercial process for removing sulfur from organosulfur compounds that are present in petroleum distillates; this involves a reaction with hydrogen gas (up to 200 atm pressure) at temperatures of 300–450 °C over a heterogeneous catalyst such as cobalt–molybdenum sulfide species supported on alumina.[3] Interestingly, despite the widespread use of HDS for many years, the mechanism of the reactions involved is still a matter of debate. In order to understand how the reactants are absorbed and react on the catalyst surface under the conditions used for HDS, the study of the reaction of thiophene and derivatives with homogeneous transition-metal complexes has been considered a good strategy.[4] Although model studies represent very different situations to those used in the commercial HDS process, the insights obtained have proven highly valuable, as summarized by Angelici in an earlier review.[5] Complexes of platinum group metals have been particularly useful to this end, showing very high HDS activity.[6]

[a] Dipl.-Chem. F. Novio, Prof. Dr. P. González-Duarte, Prof. Dr. A. Lledós, Dr. R. Mas-Ballesté
Departament de Química, Universitat Autònoma de Barcelona
08193 Bellaterra, Barcelona (Spain)
Fax: (+34) 935-813-101
E-mail: Pilar.Gonzalez.Duarte@uab.es
agusti@klingon.uab.es

Supporting information for this article is available on the WWW under http://www.chemeurj.org/ or from the author.

Outstanding features can be deduced from the various approaches developed to provide information about platinum-mediated desulfurization of thiophene (T), benzothiophene (BT) and dibenzothiophene (DBT) and related compounds. These can be summarized as follows:

1) Essentially electron-rich Pt^0 and also Pt^I complexes have been assayed
2) The first step of the HDS reaction usually leads to the insertion of platinum into the C–S bond and therefore to the formation of a six-membered thiaplatinacycle of general formula $[Pt(\eta^2\text{-}S,C\text{-}C_aH_bS)(P)_2]$ (P = phosphane; for T, $a=b=4$; for BT, $a=8$, $b=6$; for BDT, $a=12$, $b=8$).[7]
3) The presence of protonic acids causes degradation of the thiaplatinacycle without achieving desulfurization of the initially coordinated organosulfur ligand; thus, acids with noncoordinating anions give rise to cleavage of the Pt–C bond and yield dinuclear thiolate complexes of formula $[Pt_2(\mu\text{-}SR)_2P_4]^{2+}$, while the reaction with HCl cleaves both the Pt–C and Pt–S bonds to afford the very stable $[PtCl_2P_2]$ species together with thiols and/or other sulfur-containing organic compounds,[8]
4) In contrast, conversion of thiaplatinacycle over time[9] or its further reaction with various hydrides[7a,d] causes cleavage of the Pt-S-C linkage at the S–C bond thus leading to the formation of dinuclear $[Pt_2(\mu\text{-}S)_2P_4]$[9] or $[Pt_2(\mu\text{-}S)(P\cap P)_2]$,[7d] or mononuclear $[Pt(H)(SH)P_2]$ species,[7a] which evidently involve desulfurization of the organic ligand.

These platinum complexes, together with the cationic species $[Pt_2(\mu\text{-}H)(\mu\text{-}S)(P\cap P)_2]^+$ that was characterized in our lab as a result of the activation of the C–S(thiolate) bond,[10] find a parallel in Ni-mediated HDS studies in which $[Ni_2(\mu\text{-}S)_2(P\cap P)_2]$, $[Ni_2(\mu\text{-}S)(P\cap P)_2]$, and $[Ni_2(\mu\text{-}H)(\mu\text{-}S)(P\cap P)_2]^+$ have been characterized.[11]

The nature of the platinum complexes obtained as a result of the degradation of the thiaplatinacycles and subsequent desulfuration reactions attracted our attention, mainly because some of these complexes were also formed either within the cascade of reactions following the protonation of the $\{Pt_2(\mu\text{-}S)_2\}$ core[12] or by S–C cleavage in the mononuclear thiolate complex $[Pt(SR)_2(P\cap P)]$.[10] Understanding the rich chemistry of $[Pt_2(\mu\text{-}S)_2(P\cap P)_2]$ complexes has been the aim of our research for several years.[13] Now, taking advantage of the knowledge accumulated over this time, we have studied how $[Pt_2(\mu\text{-}S)_2(dppp)_2]$ (dppp = 1,3-bis(diphenylphosphanyl)propane) and other compounds that can be considered relevant to the HDS process, such as $[Pt(H)(SH)(dppp)]$, $[Pt(SH)_2(dppp)]$, $[Pt_2(\mu\text{-}S)(dppp)_2]$ and $[Pt_2(\mu\text{-}H)(\mu\text{-}S)(dppp)_2]^+$, may be interrelated, taking the cationic binuclear trihydride complex $[Pt_2(H)_2(\mu\text{-}H)(dppp)_2]^+$ as the starting point. As shown in Scheme 1 the equilibria governing their mutual interconversion as well as the corresponding reaction pathways have been analyzed. These results not only show the remarkable diversity of the reactions undergone between complexes containing Pt–H, Pt–SH, and Pt–S fragments and their strong dependence on the experimental conditions, but also provide an adequate base for further addressing studies of platinum-mediated homogeneous hydrodesulfurization reactions.

Abstract in Catalan: *La importància del platí en les reaccions del tiofè i llur derivats amb complexos de metalls de transició en fase homogènia, les quals es consideren models del procés de hidrodesulfuració, ens ha dut a l'estudi de la química de complexos que contenen els fragments Pt–H, Pt–SH i Pt–S. L'exploració de les reaccions que es desencadenen per addició de quantitats controlades de Na_2S o NaSH a $[Pt_2(H)_2(\mu\text{-}H)(dppp)_2]ClO_4$ (**1**) ha fet palesa la formació de $[Pt_2(\mu\text{-}H)(\mu\text{-}S)(dppp)_2]ClO_4$ (**2**), $[Pt(H)(SH)(dppp)]$ (**3**), $[Pt_2(\mu\text{-}S)_2(dppp)_2]$ (**4**), $[Pt_2(\mu\text{-}S)(dppp)_2]$ (**5**) i $[Pt(SH)_2(dppp)]$, on dppp representa 1,3-bis(difenilfosfanil)propà. En conseqüència, els complexos **1**, **2** i **5**, així com els anteriorment descrits **3**, **4** i $[Pt(SH)_2(dppp)]$, han estat sintetitzats i caracteritzats espectroscòpicament. També s'ha resolt l'estructura cristallina de **1** i **2**. Els complexos **1–5** constitueixen l'esquelet bàsic del conjunt de reaccions que expliquen l'evolució de **1** sota diferents condicions experimentals, com es mostra a l'Esquema 1. Aparentment, els complexos **2** and **4** constitueixen els punts morts de la xarxa de reaccions. Ara bé, la seva interconversió recíproca, mitjançant la substitució d'un lligand pont hidrur o sulfur en els respectius cores $\{Pt(\mu\text{-}H)(\mu\text{-}S)Pt\}$ i $\{Pt(\mu\text{-}S)_2Pt\}$, permet el tancament del cicle de reaccions que uneix als complexos **1–5**. Càlculs teòrics donen suport a l'existència de espècies intermediàries no detectades, les quals s'han proposat per la conversió de **1** a **2** i de **3** a **2**, i també justifiquen el comportament fluxional de **1** en solució. La naturalesa de les espècies intermediàries proposades està d'acord amb els resultats experimentals obtinguts en reaccions anàlogues amb reactius marcats isotòpicament, les quals han fet palès que **1** és la font dels lligands hidrur presents en els complexos **2** i **3**. En conjunt, els nostres resultats mostren que tant la formació dels complexos **1–5** com la seva evolució en solució són fortament dependents de les condicions experimentals.*

Results and Discussion

General description of the reactivity of complexes containing Pt–H, Pt–SH, and Pt–S fragments that are obtained from $[Pt_2(H)_2(\mu\text{-}H)(dppp)_2]ClO_4$: The set of complexes **2–5** that are obtained by the reaction of the binuclear trihydride complex $[Pt_2(H)_2(\mu\text{-}H)(dppp)_2]ClO_4$ (**1**) with Na_2S or NaHS and subsequent treatment of the resulting species with protons, hydride, hydroxide, or hydrogen sulfide ions is shown in Scheme 1. This also includes the network of reactions that have been established between these complexes. Information about the progress of each reaction was obtained through monitoring the reactions as function of time by means of NMR spectroscopy and mass spectrometry mea-

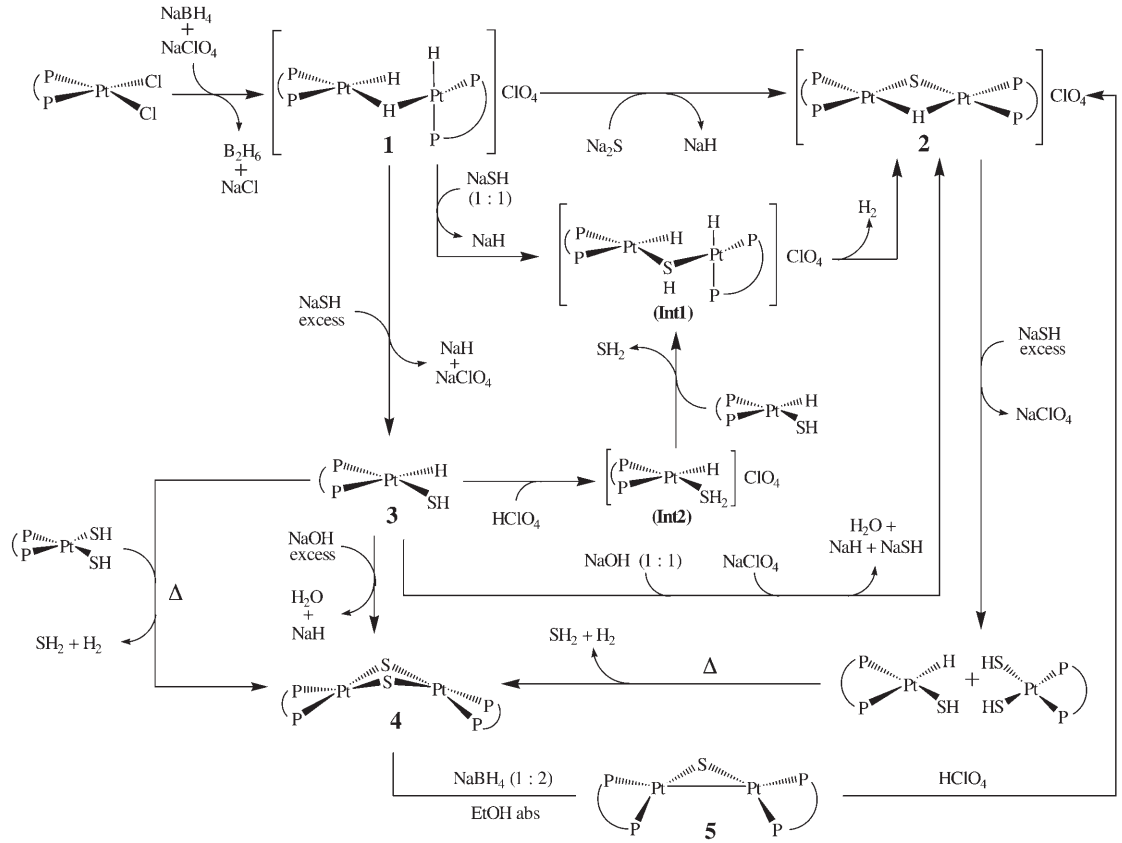

Scheme 1. Reactions pathways from **1** to **2**–**5** and corresponding interconversion reactions. All platinum complexes have been isolated and characterized. The nature of the undetected intermediate species **Int1** and **Int2** is based on theoretical calculations and it is consistent with the reactions carried out with labeled reagents.

surements. These data made it possible not only to detect and make a preliminary identification of a new complex, but also to establish the optimal conditions for its synthesis, which, in turn, enabled its full characterization. In general, the disappearance of the starting complex was concomitant with the formation of the product without detection of intermediate species. Details of all these reactions, the theoretical studies that support the undetected intermediates proposed and the results of comparable reactions carried out with labeled reagents are discussed below. Main spectroscopic data of all platinum complexes are given in Table 1. The various experimental conditions under which the reac-

Table 1. ESI MS and NMR[a] data for the platinum complexes involved in Scheme 1.

	m/z (calcd mass)	$\delta(^{31}P)$ [ppm]	$\delta(^{1}H)$ [ppm]	^{1}J(H,Pt) [Hz]	^{2}J(H,P) [Hz]	^{2}J(P,Pt) [Hz]	^{1}J(P,Pt) [Hz]	J(P,P) [Hz]	$\delta(^{195}Pt)$[b] [ppm]	Ref.
$[PtCl_2(dppp)]$	642.9 (643)[c]	−3.7	–	–	–	–	3408	–	−4505	[20]
1	1217.7 (1217)[d]	10.2	−3.67	458.8	40.0	173.6	2914	7.7	−4976[e]	[15]
2	1248.3 (1248)[d]	−6.3 (P′) −10.4 (P″)	−5.23	552.5	69.4 (P′) 8.0 (P″)	47 (P′) 28 (P″)	3684 (P′) 2702 (P″)	33,[f] 6[g] 65,[h] 0[i]	−5491	this work
3	640.9 (641)[j]	1.0 (P′) 4.0 (P″)	−3.92 (H) 0.03 (SH)	936.8	195.1 (P′) 10.7 (P″)	–	3068 (P′) 1747 (P″)	23.0	−4889	[16b]
4	1279.7 (1279)	−0.1	–	–	–	–	2615	–	−4370.5	[20]
5	1248.3[k] (1248)	−6.8 (P′) −1.3 (P″)	–	–	–	60 (P′) 28 (P″)	3147 (P′) 2288 (P″)	−28,[l] 6[m] 15,[n] 10[o]	−4315.5	this work
$[Pt(SH)_2(dppp)]$	640.1 (640)[p]	−1.30	−1.00	–	–	–	2768	–	−4791	[12b]

[a] Solvents in NMR measurements: **1**, **2**, **3** in CD_3Cl; $[PtCl_2(dppp)]$, **4**, **5**, $[Pt(SH)_2(dppp)]$ in $[D_6]$DMSO. P′ and P″ denote phosphorus atoms in *cis* or *trans* position to sulfur, respectively. [b] ^{195}Pt NMR data for all complexes is unreported. [c] Calcd mass for $[PtCl(dppp)]^+$ ion. [d] Calcd mass for the cation of the corresponding complex. [e] In CD_2Cl_2. [f] ^{2}J(P′,P″). [g] ^{3}J(P″,P″). [h] ^{3}J(P′,P′). [i] ^{3}J(P′,P″). [j] Calcd mass for $[Pt(H)(SH)(dppp)]^+$. [k] Consistent with the reaction observed for **5** with $HClO_4$, the species detected by ESI-MS corresponds to the cation of complex **2**. [l] ^{2}J(P′,P″). [m] ^{3}J(P″,P″). [n] ^{3}J(P′,P′). [o] ^{3}J(P′,P″). [p] Calcd mass for $[Pt(SH)(dppp)]^+$.

tions were monitored by NMR spectroscopy and mass spectrometry are shown in Table 2. Analogous information for the reactions involving deuterated compounds is summarized in Table 3.

Table 2. Reaction conditions and complex species formed throughout different processes at room temperature as deduced by NMR and ESI MS data.

Reagents	Solvent	Molar ratio[a]	Time [h][b]	Yield [%]	Identified species
1 + $Na_2S{\cdot}9H_2O$	C_6H_6	1:2	6	85	**2**
1 + NaSH	C_6H_6	1:1	8	70	**2**
		1:15	3	75	**3**
2 + NaSH	C_6H_6[c]	1:2	12	45	**4**
	C_6H_6	1:10	12	71	**3** + $[Pt(SH)_2(dppp)]$
2 + $HClO_4$[d]	CH_3CN	1:1		no reaction	
		1:20		no reaction	
3 + $HClO_4$[d]	CH_3CN	1:1	1	80	**2**
		1:10	0.25	68	**2**
3 + NaOH[e]	CH_3CN	1:1	2	72	**2**
3 + NaOH[f]	CH_3CN	1:10	2	70	**4**
3 + $[Pt(SH)_2(dppp)]$	C_6H_6[c]	1:1	12	63	**4**
4 + $NaBH_4$	EtOH abs.	1:4	6	85	**5**
5 + $HClO_4$[d]	CH_3CN[g]	1:1.5	2	74	**2**

[a] Platinum complex to reagent molar ratio. [b] Reaction time for maximum yield. [c] Reflux temperature. [d] 12 M $HClO_4$. [e] 2 M NaOH. [f] 4 M NaOH. [g] The same results are obtained in EtOH solvent.

Table 3. Ancillary reactions with deuterated reagents monitored by ^{31}P, ^{1}H, and ^{2}H NMR: experimental conditions and corresponding products.

Reagents[a]	Solvent	Molar ratio[b]	Time [h][c]	Identified species	Yield[d] [%]
1d + Na_2S	C_6H_6	1:2	6	[D]**2d**	86
1 + Na_2S + D_2O	C_6H_6	1:2	6	pure **2**	0
1d + NaSH	C_6H_6	1:1	8	[D]**2d**	78
		1:15	3	[D]**3d**	82
3d + $HClO_4$[e]	CH_3CN	1:1	1	[D]**2d**	79
		1:10	0.25	[D]**2d**	71
3d + NaOH[f]	CH_3CN	1:1	2	[D]**2d**	80
2d + H_2O	CH_3CN	1:20		no reaction	
2 + D_2O	CH_3CN	1:20		no reaction	

[a] Details of the synthesis of **1d**–**3d** as well as their main ^{1}H and ^{2}H NMR features are given in the Experimental Section. All reactions were performed at room temperature. [b] Platinum complex to reagent molar ratio. [c] Reaction time for complete disappearance of the starting platinum complex. [d] The percentage of moles of deuterated species with respect to the sum of deuterated and non deuterated compound. In all reactions the deuterium transferred from the reagent to the product is within the range of 87–98 %. [e] 12 M $HClO_4$. [f] 2 M NaOH.

Complex **1** was synthesized in high yields by using a one-pot reaction procedure that involves the mixing of $[PtCl_2(dppp)_2]$ and $NaBH_4$ at a 1:2 molar ratio in ethanol at room temperature and the subsequent addition of $NaClO_4$. The same procedure with $NaBD_4$ at a 1:4 molar ratio afforded the deuterated analogue **1d** in 72 % yield. On the basis of ^{1}H and ^{2}H NMR data complex **1d** encloses an isotopic mixture of the $\{PtD_3Pt\}$, $\{PtD_2HPt\}$, and $\{PtDH_2Pt\}$ fragments in 75:15:10 molar ratios (see Experimental Section). This data shows that the resulting stoichiometry for the core of **1d** is $\{Pt_2D_{2.65}H_{0.35}\}$, or that the deuterium to hydrogen content in this complex is 88:12.

The synthetic procedure we followed to obtain **1** has already been reported for the $[Pt_2(H)_3(dcype)_2]X$ (dcype = 1,2-bis(dicyclohexylphosphanyl)-ethane; X = BF_4, Cl, OH, and BPh_4) analogues,[14] and affords much better yields than the two synthetic alternatives used to obtain $[Pt_2(H)_3(dppp)_2]BF_4$,[15] which includes the same diphosphane ligand as **1**. Addition of the sodium salts of BF_4^-, BPh_4^-, or PF_6^- instead of ClO_4^- led us to unsatisfactory yields, and that of Cl^- reversed the reaction by causing formation of the starting complex $[PtCl_2(dppp)]$. The X-ray structure of the binuclear trihydrido cation of **1** and the theoretical calculations that account for its fluxional behavior in solution are described in the next section.

The reaction of **1** with $Na_2S{\cdot}9H_2O$ at a 1:2 molar ratio in benzene solution (Table 2), or alternatively with anhydrous Na_2S in the presence of D_2O (Table 3), affords **2** in high yield, the X-ray structure of which, described below, has enabled identification of the unusual $\{Pt(\mu\text{-}H)(\mu\text{-}S)Pt\}$ core. To ascertain the source of the bridging hydrogen ligand in **2**, complex **1** was replaced by **1d** in the reaction with anhydrous Na_2S (Table 3). On the basis of NMR data, the product thus obtained includes a $\{Pt(\mu\text{-}D)(\mu\text{-}S)Pt\}$ core and corresponds to the deuterated analogue [D]**2d**, which remains unaffected after addition of water. These results show that the $\{Pt_2H_3\}$ core in complex **1** is the only source of the bridging hydride ligand in the $\{Pt(\mu\text{-}H)(\mu\text{-}S)Pt\}$ core of **2**. Despite its remarkable stability in the solid phase and in solution even in the presence of acids or bases, the only precedents of this core reduce to $[Pt_2(\mu\text{-}H)(\mu\text{-}S)(dppe)_2]^+$ (dppe = 1,2-bis(diphenylphosphanyl)ethane)[10] and $[Ni_2(\mu\text{-}H)(\mu\text{-}S)(dippe)_2]^+$ (dippe = 1,2-bis(diisopropylphosphanyl)-ethane).[11] However, the formation of $[Pt_2(\mu\text{-}H)(\mu\text{-}S)(dppe)_2]^+$ was due to the result of a serendipitous preparation and the presence of the bridging sulfide was attributed to the S–C bond cleavage of the aminothiolate ligand in the starting complex $[Pt(SC_5H_9NMe)_2(dppe)]$. On the one hand, the synthesis reported here for **2** provides a reproducible method to obtain the $\{Pt(\mu\text{-}H)(\mu\text{-}S)Pt\}$ core with phosphine terminal ligands. On the other hand, the corresponding spectroscopic parameters enable identification of the formation of such a core as the result of reactions that may involve activation of the S–C bond.

Another method for obtaining **2** from **1** is reaction with NaSH at a 1:1 molar ratio. Monitoring of this reaction by ^{31}P and ^{1}H NMR spectroscopy gave no evidence of inter-

mediate species and thus formation of known mononuclear complexes such as **3** and/or $[Pt(SH)_2(dppp)]$[12a] was discarded. On this basis, it seems reasonable to propose the pathway shown in Scheme 1, the first step of which would consist of the substitution of a bridging hydride in **1** by the hydrogensulfide anion. Then, the intermediate $[Pt_2(H)_2(\mu\text{-}SH)(dppp)_2]^+$ (**Int1**) thus formed would convert rapidly into **2**. This could occur by means of an intramolecular acid–base reaction between one remaining terminal hydride ligand and the proton of the SH^- group. On the one hand, this proposal is consistent with the results obtained in the reaction of **1d** with NaSH at a 1:1 molar ratio. This reaction affords **2d** (Table 3) and thus shows that the $\{Pt_2H_3\}$ core and not the hydrogensulfide anion is the source of the bridging hydrogen ligand in **2**. On the other hand, thermodynamic viability of this proposal has been corroborated by the theoretical calculations discussed below.

Interestingly, if complex **1** is treated with excess NaSH, instead of a 1:1 molar ratio, the reaction affords **3** in high yield, a mononuclear platinum(II) complex, which, on the basis of NMR data, contains the {Pt(SH)(H)} fragment. It is also remarkable that the reaction of **1d** with excess NaSH yields the [D]**3d** analogue that contains the {Pt(SH)(D)} fragment (Table 3). Under inert atmosphere complex **3** is highly stable not only in the solid phase, but also in benzene at reflux temperature. This stability indicates that although both H^- and SH^- ligands are bound to the same platinum atom they do not undergo the intramolecular acid–base reaction that could lead to **4** by the mechanism proposed above for the conversion of the intermediate $[Pt_2(H)_2(\mu\text{-}SH)(dppp)_2]ClO_4$ species. Notwithstanding this stability, our attempts to obtain single crystals of **3** were unsuccessful. This is consistent with the fact that while complexes of the same formula have been synthesized as a result of the oxidative–addition reaction of SH_2[16] or thiophene[7a] to zerovalent platinum compounds or by the reaction of chloro complexes of Pt^{II} with NaSH,[17] their X-ray structures are unreported. Under open atmosphere, the monitoring of solutions of **3** by ^{31}P NMR spectroscopy and ESI MS shows the slow appearance of the dinuclear complex **2**.

The stability of **3** under inert atmosphere contrasts with the richness of its chemistry in the presence of acids or bases, which probably stems from the amphoteric behavior of the SH ligand bound to platinum. Thus, **3** reacts with both $HClO_4$ and NaOH, and in the latter case, depending on the complex to base molar ratio, the reaction affords different products.

The reaction of **3** with $HClO_4$ in acetonitrile yields **2** quantitatively. Monitoring this reaction by ^1H and ^{31}P NMR spectroscopy, we were unable to detect any intermediate species. However, the reactions of **3d** with $HClO_4$ at 1:1 and 1:10 molar ratio afforded **2d** (Table 3), which is consistent with the protonation of the SH group and its subsequent leaving as an SH_2 compound. These results and theoretical calculations showing that in **3** the hydrogensulfide ligand is more basic than the hydride together with other theoretical data described below are consistent with the three-step pathway depicted in Scheme 1. The first involves the protonation of the SH ligand in **3** to give the unknown $[Pt(H)(SH_2)(dppp)]^+$ ion (**Int2**), then this species rapidly dimerizes with the remaining unprotonated fraction of **3** to afford the intermediate $[Pt_2(H)_2(\mu\text{-}SH)(dppp)_2]ClO_4$ (**Int1**) complex, which eventually converts into **2**. The first two steps are corroborated by the reaction of **3** with HCl instead of $HClO_4$. Therefore, the slow addition of one equivalent of HCl to **3** enables identification of the already known [PtCl(H)(dppp)] complex[18] as an intermediate species in the reaction that eventually leads to **2**. Formation of [PtCl(H)(dppp)] can be attributed to the binding properties of the chloride ion, which, unlike ClO_4^-, causes the replacement of SH_2 in the $[Pt(H)(SH_2)(dppp)]^+$ cation. The subsequent conversion of [PtCl(H)(dppp)] could take place in accordance with the reported reaction between $[PtCl(H)(PEt_3)_2]$ and $[Pt(H)(SH)(PEt_3)_2]$, which affords $[(PEt_3)_2Pt(H)(\mu\text{-}SH)(H)Pt(PEt_3)_2]^+$.[19] The reason why this last complex has been isolated, while its dppp analogue has been undetected, and presumably converts into **2** with the concomitant release of H_2, must be related to the different nature of the phosphane ligands. In contrast to the slow reaction with moderate amounts of HCl, the fast addition of excess HCl to **3** immediately leads to the starting $[PtCl_2(dppp)]$ complex.

The reaction of **3** with NaOH in acetonitrile shows exceptional features as it leads to **2** if performed at a 1:1 molar ratio, but to **4** with excess NaOH (1:10), in both cases with high yields (about 70%). The monitoring of these reactions by NMR spectroscopy and ESI MS provides no evidence of intermediate species, but shows that the disappearance of **3** is concomitant with the formation of either **2** or **4**, depending on the reaction conditions. The spectroscopic data of the former is described in this work and those of the latter, already obtained by the reaction of $[PtCl_2(dppp)]$ with $Na_2S{\cdot}9H_2O$, have been reported elsewhere.[20] On the basis of DFT calculations the proposed reaction pathways from **3** to either **2** or **4** are shown in Scheme 2. The first step, which involves deprotonation of the SH ligand in **3**, is common in both pathways. From this stage there are two possibilities. In one, the intermediate $[Pt(H)(S)(dppp)]^-$ species reacts with itself, which occurs in the reaction where excess of NaOH is present. In the other pathway the $[Pt(H)(S)(dppp)]^-$ species reacts with **3** as in this case the amount of base added has enabled deprotonation of only a fraction of the initial complex. The reaction of two $[Pt(H)(S)(dppp)]^-$ species to yield **4** probably involves the nucleophilic attack of each sulfide ligand to the platinum center of the other species, which causes displacement of the two initially bound hydride anions. In contrast, the formation of **2** would involve the nucleophilic attack of the sulfide ligand in $[Pt(H)(S)(dppp)]^-$ to the platinum center in **3**, this being followed by the leaving of one hydrogensulfide and one hydride anion.

To obtain **4**, an alternative procedure to the addition of excess NaOH to **3** is the reaction of this complex with $[Pt(SH)_2(dppp)]$ in benzene at reflux temperature. The synthesis and X-ray structural characterization of compound **4**, which we identified within the set of reactions following the

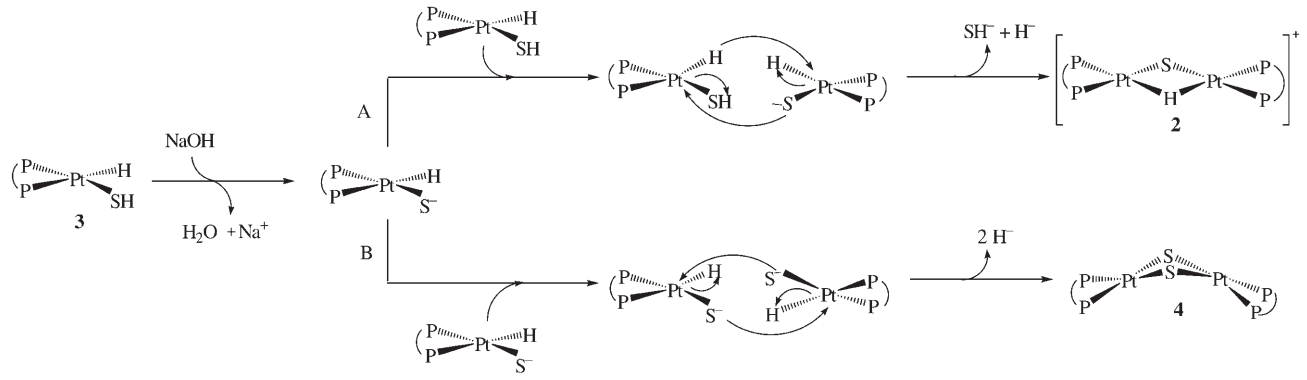

Scheme 2. Reaction pathways proposed for the reaction of **3** with NaOH at 1:1 (A) and 1:10 (B) molar ratio.

protonation of the $\{Pt_2S_2\}$ core, have already been reported.[12b] Significantly, analogue complexes such as *cis*-$[Pt(SH)_2(PPh_3)_2]$ have been described as homogeneous catalysts in model studies for the Claus process,[21] in which the SH_2 generated in HDS reacts with SO_2 over alumina at 300 °C to give sulfur and water.

A perspective view of the reactions described up to this point could easily suggest that complexes **2** and **4** are the dead ends of the system studied. Within this context, the mutual interconversion of the $\{Pt(\mu\text{-}H)(\mu\text{-}S)Pt\}$ and $\{Pt(\mu\text{-}S)_2Pt\}$ cores posed us with a challenge. Exploration of the chemistry involved in the replacement of one bridging hydride or sulfide ligand in the dinuclear complexes **2** and **4**, respectively, provided unprecedented results and enabled the closure of an otherwise open cycle.

Treatment of **2** with slight excess of NaSH (1:2 molar ratio) in benzene at room temperature gives no reaction, but yields **4** quantitatively if the mixture is heated at reflux temperature. To elucidate the influence of the amount of NaSH and temperature in this reaction, **2** was treated with a great excess of NaSH in benzene at room temperature and the reaction monitored by ^1H and ^{31}P NMR spectroscopy. This data provided evidence for the complete conversion of **2** into an equimolar mixture of **3** and $[Pt(SH)_2(dppp)]$. Heating the resulting solution at reflux temperature yielded **4**, as expected on the basis of the data obtained in the synthesis of **4** from **3** and $[Pt(SH)_2(dppp)]$.

Analogously to the evolution from **2** to **4**, the reverse reaction also occurs in two steps, as the reaction of **4** with excess $NaBH_4$ in absolute ethanol at room temperature affords the unreported dinuclear complex **5** with very high yield. Its relatively low stability over time, even under inert atmosphere, probably accounts for the difficulties encountered for obtaining single crystals. Consistently, not one X-ray structure of complexes of formula $[Pt_2(\mu\text{-}S)L_4]$, L = phosphane, has been reported. Complex **5** has been spectroscopically characterized and its NMR parameters are consistent with data in the literature as discussed below. In addition, closely related species have been obtained in model studies of HDS with nickel and platinum complexes.[11,7d] Overall, the use of $NaBH_4$ made it possible to establish an unprecedented path in order to achieve the reductive desulfurization of a $\{Pt_2S_2\}$ core and therefore the formation of a Pt–Pt bonded $\{Pt_2^{I}S\}$ triangle, the only precedent for which refers to the reaction of $[Pt_2(\mu\text{-}S)_2(PPh_3)_4]$ with CO.[22] However, **4** did not react with CO at various temperatures and pressures, possibly because the bidentate phosphane ligands do not facilitate the coordination of CO to platinum as terminal ligand, as proposed in the mechanism for the reduction of $[Pt_2(\mu\text{-}S)_2(PPh_3)_4]$. Concerning the synthesis of **5**, the evolution from $\{Pt_2S_2\}$ to a $\{Pt_2S\}$ core by reaction with $NaBH_4$ is remarkable as this reagent usually causes either reduction of Pt^{II} to Pt^0,[23] or cluster degradation, as shown in its reaction with $\{M_3S_2\}$ aggregates to afford $\{M_3S\}$ clusters.[24] On this basis, it appears that the bidentate chelating dppp ligand plays a significant role in the specificity of the reducing agent to yield **5** as well as in the stabilization of Pt^{I} in this complex.

In a subsequent step, the addition of $HClO_4$ to **5** in either ethanol or acetonitrile afforded **2**, which was easily identified on the basis of the NMR and ESI MS data given in Table 1. This synthetic procedure has precedents in the reaction of $[Ni_2(\mu\text{-}S)(dippe)_2]$ with HPF_6 that affords $[Ni_2(\mu\text{-}H)(\mu\text{-}S)(dippe)_2]^+$,[11] already mentioned as one of the few examples of complexes with a $\{M_2(\mu\text{-}H)(\mu\text{-}S)\}$ core.

Spectroscopic and structural characterization of complexes 1–5: All reactions depicted in Scheme 1 were monitored by means of multinuclear NMR (^1H, ^{31}P, ^{195}Pt) spectroscopy and ESI mass spectrometry (MS). Owing to the unique $^{31}P\{^1H\}$ NMR spectral features of the complexes involved, this technique was the main tool used to detect their formation. However, full characterization of the species identified by using this technique requires knowledge of additional structural and spectroscopic data. To this end, the synthesis and spectroscopic characterization of complexes **1–5**, $[PtCl_2(dppp)]$ and $[Pt(SH)_2(dppp)]$ were undertaken. Those of **2** and **5** together with the ^{195}Pt NMR parameters for all the complexes are unprecedented. These are given in Table 1 and are discussed below. However, the same cationic complex as that found in **1** had already been reported as the tetrafluoroborate salt.[15] Spectroscopic data for compounds **1**,[15] **3**,[16b] **4**,[20] $[PtCl_2(dppp)]$[20] and $[Pt(SH)_2(dppp)]$[12b] were fully consistent with previously reported data for these com-

plexes. Concerning the structural parameters in the solid phase, the X-ray structures of **1** and **2** are described below and that of **4**,[20] $[PtCl_2(dppp)]$[25] and $[Pt(SH)_2(dppp)]$[12b] are already known. The main NMR and ESI-MS parameters for complexes **1**–**5**, $[PtCl_2(dppp)]$ and $[Pt(SH)_2(dppp)]$ are summarized in Table 1.

Regarding complex **1**, it is worth noting that the high symmetry observed in the proton, phosphorus, and platinum NMR spectra is not consistent with the crystal structure. This apparent discrepancy is the result of a fluxional behavior for bridging and terminal hydrido ligands in the $[Pt_2(H)_2(\mu\text{-}H)(dppp)_2]^+$ ion, as already reported.[15] Both, the crystal structure of **1** and the theoretical calculations that account for this dynamic process are discussed below.

The ^1H, ^{31}P, and ^{195}Pt NMR features of **2** provide relevant information about its structure in solution and compare well with those reported for the analogues $[Pt_2(\mu\text{-}H)(\mu\text{-}S)(dppe)_2]^+$[10] and $[Pt_2(\mu\text{-}H)(\mu\text{-}CO)(P\cap P)_2]^+$ (P∩P = dppe, dppp, dppb; dppb = 1,4-bis(diphenylphosphanyl)butane),[26] the latter at low temperature. The ^1H, $^1H\{^{31}P\}$ and $^{31}P\{^1H\}$ spectra are depicted in Figures 1 and 2. The $^1H\{^{31}P\}$ spectrum in the high-field region (Figure 1a) displays a pseudo-quintet structure centered at −5.22 ppm arising from coupling ^1J(H,Pt) (552 Hz) to two equivalent Pt atoms. This unambiguously demonstrates the presence of a bridging hydrogen atom between two PtP_2 units. In the ^1H spectrum (Figure 1b) each of these signals is split into a triplet of triplets, owing to the coupling of this hydrogen atom with the phosphorus nuclei located in *trans* (P′) and *cis* (P″) positions (^2J(H,P′) = 69 Hz, ^2J(H,P″) = 8 Hz). The two non-equivalent sets of phosphorus nuclei become evident in the $^{31}P\{^1H\}$ spectrum (Figure 2a), which displays an unsymmetrical second-order pattern characteristic of bimetallic species containing two $\{Pt^{II}(P\cap P)\}$ moieties. It therefore shows two distinct signals centered at $\delta = -6.3$ (^1J(P′,Pt) = 3684 Hz) and $\delta = -10.4$ ppm (^1J(P″,Pt) = 2702 Hz), respectively, and observed as an apparent doublet of doublets. However, full interpretation of this spectrum requires consideration of J(P,Pt) and J(P,P) couplings through the platinum-platinum axis.[26] On this basis, the values ^2J(P′,Pt) = 47, ^2J(P″,Pt) = 28, ^2J(P′,P″) = 33, ^3J(P′,P′) = 65 and ^3J(P″,P″) = 6 Hz were obtained. The good match between the experimental and simulated spectra is shown in Figure 2b. The difference between the two ^1J(P,Pt) and the two ^2J(P,Pt) provides evidence of the distinct *trans* influence of the bridging ligands, S^{2-} and H^-. ^1H,^1H NOE and ^{31}P,^1H HMBC experiments meant we could establish that the bridging hydride is located in *cis* position with respect to P″ and therefore that the *trans* influence follows the order: $S^{2-} > H^-$. On this basis, the highest ^1J(P,Pt) and ^2J(P,Pt) values were assigned to the couplings with the phosphorus atoms *cis* to sulfur as shown in Table 1. As expected, the NMR parameters found for **2** are similar to those reported for the $[Pt_2(\mu\text{-}H)(\mu\text{-}S)(dppe)_2]^+$[10] analogue, but are significantly different from those for $[Pt_2(\mu\text{-}H)(\mu\text{-}CO)(dppp)_2]^+$.[26] Comparison of the ^1J(P″,Pt) values in the three complexes is consistent with the following order of *trans* influence for the bridging ligands: $CO > S^{2-} > H^-$, as the ^1J(P″,Pt) value in **2** is greater than in the CO analogue. The presence of the hydride bridge in **2** is confirmed in the ^{195}Pt spectrum and corroborated by X-ray data in the solid phase. Concerning variable-temperature (VT) NMR data for **2**, all features remained unaltered throughout the temperature range −70 to +120 °C, which provides evidence for the stereochemical rigidity of the $\{Pt(\mu\text{-}H)(\mu\text{-}S)Pt\}$ core in contrast to the dynamic properties shown by complexes $[Pt_2(\mu\text{-}H)(\mu\text{-}CO)(P\cap P)_2]^+$ (P∩P = dppe, dppp, dppb) in solution.[26]

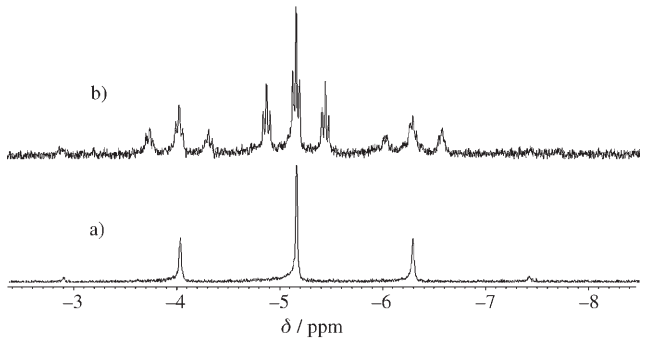

Figure 1. ^1H NMR high-field region for **2** in $CDCl_3$ solvent: a) $^1H\{^{31}P\}$ and b) ^1H NMR.

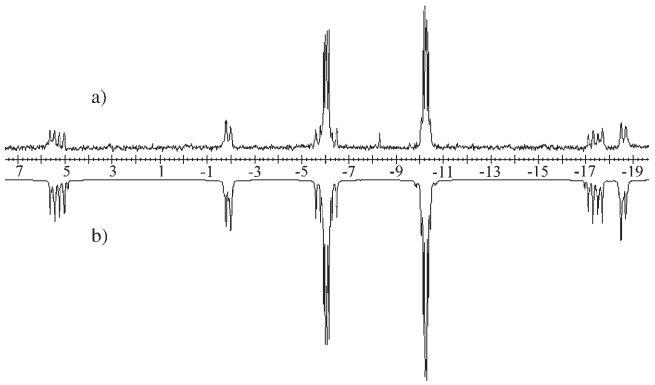

Figure 2. $^{31}P\{H\}$ NMR spectra of **2**: a) experimental spectrum in $CDCl_3$ and b) the corresponding computer simulation.

The structural information obtained from NMR data for **2** is consistent with the ESI MS spectrum with a major peak at $m/z = 1248.3$, which corresponds to the molecular weight of the $[Pt_2(\mu\text{-}H)(\mu\text{-}S)(dppp)_2]^+$ ion. Overall, NMR and MS data are clearly indicative of its presence in solution with a similar structure to that found for the $[Pt_2(\mu\text{-}H)(\mu\text{-}S)(dppp)_2]^+$ ion in the solid phase by X-ray diffraction.

While the spectroscopic data that makes it possible to identify complexes **3** and **4** are reported elsewhere,[16b,20] characterization of complex **5** is unprecedented. This complex displays a very similar $^{31}P\{^1H\}$ spectrum (Figure 3a) to that observed for bimetallic complexes containing the $\{Pt^I{}_2S\}$ core,[27] the pattern of which is typical of a second-order

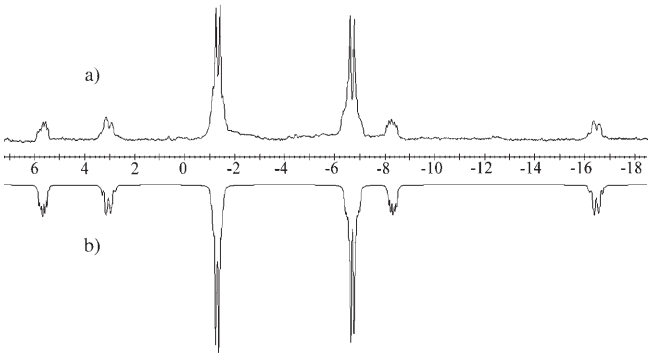

Figure 3. $^{31}P\{H\}$ NMR spectra of (**5**); a) experimental spectrum in $[D_6]DMSO$; b) the corresponding computer simulated spectrum.

spectrum. Therefore, the two distinct resonances for the phosphorus nuclei in **5** are observed as apparent doublets centered at $\delta = -1.3$ ($^1J(P,Pt) = 2260$ Hz) and -6.8 ppm ($^1J(P,Pt) = 3161$ Hz). These data, together with $^2J(P,P)$ and the sets of $^3J(P,P)$ and $^2J(P,Pt)$ couplings found for **2** (Table 1) as initial values in the computer program, enabled a good simulation of the $^{31}P\{^1H\}$ spectrum of **5** (Figure 3b). According to this simulation, $^3J(P',P')$ and $^3J(P',P'')$ in **5** have a positive sign, while $^2J(P',P'')$ has a negative sign; and the signs of these three coupling constants are independent of those of the remaining couplings. The two different values found for $^1J(P,Pt)$ and $^2J(P,Pt)$ clearly indicate a different *trans* environment for each of the two sets of equivalent phosphorus nuclei, P′ and P″. The assignment of the highest J values to the P–Pt bond involving the phosphorus nuclei *trans* to sulfur, $^1J(P'',Pt) = 3161$ and $^2J(P'',Pt) = 60$ Hz (Table 1), is based on data in the literature for related compounds.[27] Additional ^{195}Pt NMR data not only corroborate the presence of the $\{Pt^I_2S\}$ core, but also the absence of hydride ions as terminal or bridging ligands, which is fully confirmed in the ^1H and HMBC Pt,H NMR spectra. The lack of terminal hydride ligands in the solid complex **5** is consistent with the absence of a broad absorption around 2000 cm^{-1} in the infrared spectrum. ESI-MS under acidic conditions (see Experimental Section) shows a major peak at $m/z = 1248.3$, which is exactly the same value as that observed for complex **2**. This observation is fully consistent with the reactivity of **5** with protic acids, which gives **2**. Overall, the whole set of spectroscopic data lead us to propose that complex **5** corresponds to a Pt^I species of formula $[Pt_2(\mu\text{-}S)(dppp)_2]$ with a single sulfide bridge and a Pt–Pt bond. Interestingly, this bridging sulfide moiety is a common structural feature of homogeneous desulfurization products previously found for thiophene and benzothiophene substrates.[7d,11]

To further characterize complexes **1**–**5**, $[PtCl_2(dppp)]$ and $[Pt(SH)_2(dppp)]$, and therefore corroborate the interpretation of ^1H and ^{31}P NMR spectra, a study was made of their ^{195}Pt NMR parameters, including Pt–H correlation experiments for **1**–**3** and $[Pt(SH)_2(dppp)]$ (Table 1).

The $^{195}Pt\{^1H\}$ NMR spectra of complexes $[PtCl_2(dppp)]$ and $[Pt(SH)_2(dppp)]$ share common features as both display a triplet centered at $\delta = -4505$ and -4791 ppm, respectively, due to the coupling of platinum with two equivalent phosphorus nuclei. For the latter complex, this pattern converts into a triplet of triplets in the non-H-decoupled ^{195}Pt spectrum owing to couplings $^2J(H(SH),Pt) = 48.5$ Hz, thus confirming the binding of two SH groups to platinum. The dinuclear complexes **1** and **4** are symmetrical and therefore the two platinum as well as the four phosphorus nuclei are chemically equivalent. Accordingly, the triplet signal in the $^{195}Pt\{^1H\}$ NMR spectra, centered at $\delta = -4976$ (**1**) and -4370 ppm (**4**), is due to the $^1J(Pt,P)$ coupling of each platinum with two phosphorus nuclei. In the non-H-decoupled ^{195}Pt spectrum of **1**, all the peaks observed in the $^{195}Pt\{H\}$ spectrum split into quartets ($^1J_{Pt,H} = 459$ Hz), which makes it possible to unequivocally establish that the number of equilibrating hydrido ligands is three. For both **1** and **4**, the pattern of the ^{195}Pt spectra compares well with the respectively related $[Pt_2(H)_3(dppe)_2]^+$[15] and $[Pt_2(\mu\text{-}SR)_2(dppe)_2]$[28] complexes.

The $^{195}Pt\{H\}$ NMR spectrum of the unsymmetrical mononuclear complex **3** is simple and well defined, displaying a doublet of doublets owing to coupling of platinum with two non-equivalent phosphorus nuclei. The non-H-decoupled ^{195}Pt spectrum exhibits a 16-line pattern arising from $^2J(H(SH),Pt) = 63.4$ Hz and $^1J(H,Pt)$ couplings (Table 1). These values are fully consistent with those obtained from the corresponding ^1H and ^{31}P spectra, which are given in Table 1. Complexes **2** and **5** show a similar $^{195}Pt\{H\}$ NMR spectrum; in both cases the resonance of the two equivalent platinum atoms ($\delta = -5491$ (**2**), -4315 ppm (**5**)) is split by coupling to the phosphorus either in *trans* or *cis* positions to the sulfide ligand. As a result of this coupling, the spectrum has four peaks that are observed as a doublet of doublets. However, the broadness of the signals do not enable corroboration of the $^2J(P,Pt)$ values obtained for **2** and **5** from the corresponding $^{31}P\{H\}$ NMR spectrum. The $^1J(H,Pt)$ coupling observed in the non-H-decoupled ^{195}Pt spectrum of **2** unambiguously confirms the presence of a hydrido bridge, as it exhibits eight peaks of equal intensity corresponding to a doublet of double doublets. The $^1J(H,Pt)$ value is consistent with that calculated from the ^1H and $^1H\{^{31}P\}$ spectra of **2** and also with previously reported data for $[Pt_2(\mu\text{-}H)(\mu\text{-}S)(dppe)_2]^+$.[10]

Overall, the chemical shift values found for platinum in complexes **1**–**5**, $[PtCl_2(dppp)]$ and $[Pt(SH)_2(dppp)]$ (Table 1) suggest that they can be organized into three groups. Thus, dinuclear platinum complexes with only sulfide ions as bridging ligands exhibit the highest values ($\delta \approx -4350$ ppm). These are followed by the mononuclear complexes containing Cl, SH and/or H as terminal ligands ($-4900 \leq \delta \leq -4500$ ppm). The smallest values are shown by the dinuclear complexes with hydride ions as bridging ligands ($\delta \leq -4950$ ppm). It is worth noting the similarity between the chemical shift values found for complexes **4** (-4370.5 ppm) and **5** (-4315.5 ppm) despite the different oxidation state of

the platinum atoms, which is consistent with values in the literature.[10,26]

Molecular structures

*Crystal Structure of [(dppp)Pt(H)$_2$(μ-H)Pt(dppp)]ClO$_4$ (**1**)*: The structure of **1** consists of dinuclear [(dppp)Pt(H)$_2$(μ-H)Pt(dppp)]$^+$ ions (Figure 4) and ClO_4^- counterions held together by electrostatic interactions, and solvent molecules. Selected bond angles and distances are given in Table 4. The good quality of the crystal made it possible to unequivocally locate the hydride ligands. The overall geometry of the Pt_2H_3 core in **1** compares well with that previously found by neutron diffraction studies for the $[Pt_2H_3(dppe)_2]^+$ analogue.[29] The main difference between the structures containing dppp or dppe arises from the diverse values of the bite angles, which are characteristic of each diphosphane ligand. To compensate for the increase in the P-Pt-P angles in **1** (94.5 and 95.5°) with respect to its dppe analogue (86.1, 86.2°), the H-Pt-H angles involving the two central hydride ligands decrease significantly (for **1**: 69.1 and 87.2°; for its dppe analogue: 75.53 and 91.55°) with the concomitant shortening of the H···H distance (for **1**: 2.21 Å; for its dppe analogue: 2.40 Å).

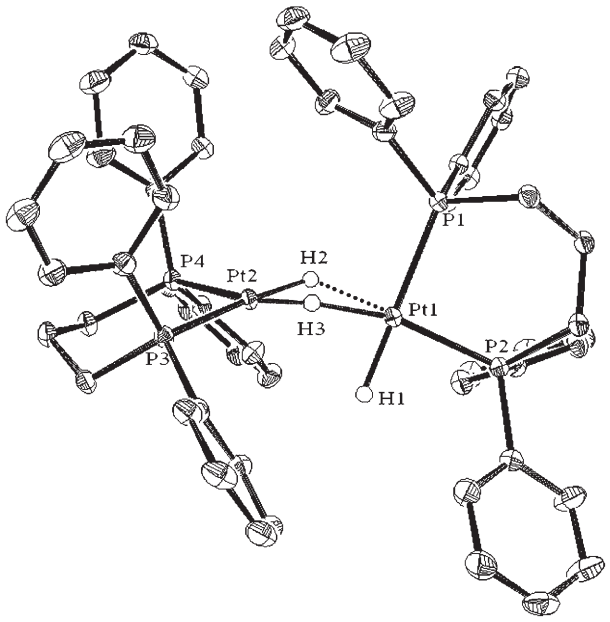

Figure 4. Structure of the cation in complex **1** with 50% probability displacement ellipsoids and selected atoms labels. H atoms are omitted except for those in the {PtH(μ-H)PtH} core.

To account for the structure of the highly unsymmetrical $\{Pt_2H_3\}$ core in **1** it could be considered as resulting from the contribution of the three connectivity models depicted in Scheme 3. Their examination reveals that the coordination geometry for one of the platinum centers (Pt2) can be described as square-planar (maximum deviation from planarity 0.09 Å) with two hydride ligands showing short Pt2–H distances (1.58 and 1.64 Å). Differences between the models proposed arise from consideration of how many hydride ligands coordinated to Pt2 are also bound to the second platinum center, the so-called Pt1.

The $\{Pt_2H_3\}$ core in model **A** can be described as a donor–acceptor complex in which the [(dppp)(Pt2)H$_2$] moiety acts as a hydride donor towards an acceptor $[(dppp)(Pt1)H]^+$ ion. According to this model, the geometry of Pt1 should be considered T-shaped (P-Pt1-H angle of 176.5°), with a very short Pt1–H distance indicating that this hydrogen atom behaves like a purely terminal hydride ligand (1.56 Å). However, the hydrides belonging to the [(dppp)(Pt2)H$_2$] moiety are at significantly long distances (2.07 Å and 1.84 Å) with respect to Pt1. These large values suggest a weak nonbonding interaction between Pt1 and the supposedly bridging hydride ligands, and therefore, for the significance of model **A**. However, if we consider that these distances are compatible with two Pt1–H bonds, the structure could be described as being formed by a [(dppp)-(Pt1)H$_3$] moiety with a very distorted trigonal bipyramidal coordination geometry ($\tau = 0.56$)[30] that shares two hydride ligands with the square-planar [(dppp)(Pt2)H$_2$] fragment (model **B**). In contrast, if the Pt1–H distance of 1.84 Å is interpreted as a bonding distance, but 2.07 Å is considered too long for a chemical bond, the structure of the $\{Pt_2H_3\}$ aggregate should be described on the basis of model **C**. In this case, one bridging hydride ligand connects two square-planar

Table 4. Selected bond lengths [Å] and angles [°] for complex **1**. In brackets are the calculated values for **1t**.

P1–Pt1	2.313(4)	[2.416]	Pt1–H3	1.84(3)	[1.799]
P2–Pt1	2.222(4)	[2.279]	Pt1–Pt2	2.70983(14)	[2.850]
P3–Pt2	2.269(4)	[2.387]	Pt2–H2	1.58(4)	[1.608]
P4–Pt2	2.250(4)	[2.308]	Pt2–H3	1.64(3)	[1.711]
Pt1–H1	1.56(3)	[1.584]	H2···H3	2.215	[2.359]
Pt1–H2	2.07(4)	[2.337]			
H1-Pt1-H2	88.4(16)	[87.7]	P1-Pt1-Pt2	104.673(11)	[98.9]
H1-Pt1-H3	86.5(16)	[87.2]	H2-Pt2-H3	87.2(17)	[90.6]
H1-Pt1-P2	84.00(13)	[85.3]	H2-Pt2-P3	175.0(13)	[177.8]
H1-Pt1-P1	176.5(13)	[179.9]	H2-Pt2-P4	88.8(13)	[88.3]
H1-Pt1-Pt2	76.5(13)	[81.0]	H2-Pt2-Pt1	49.4(13)	[55.1]
H2-Pt1-H3	69.1(14)	[68.1]	H3-Pt2-P3	88.8(12)	[87.3]
H2-Pt1-P2	139.0(10)	[132.9]	H3-Pt2-P4	172.7(12)	[177.6]
H2-Pt1-P1	90.8(10)	[92.2]	H3-Pt2-Pt1	41.5(12)	[36.8]
H2-Pt1-Pt2	35.5(10)	[34.3]	P3-Pt2-P4	95.454(16)	[93.9]
H3-Pt1-P2	149.7(10)	[157.2]	P3-Pt2-Pt1	125.78(11)	[122.7]
H3-Pt1-P1	96.4(10)	[92.8]	P4-Pt2-Pt1	136.639(11)	[142.5]
H3-Pt1-Pt2	36.3(11)	[34.7]	Pt2-H3-Pt1	102.23	[108.6]
P2-Pt1-P1	94.50(16)	[94.7]	Pt2-H2-Pt1	95.44	[90.6]
P2-Pt1-Pt2	159.355(12)	[161.3]			

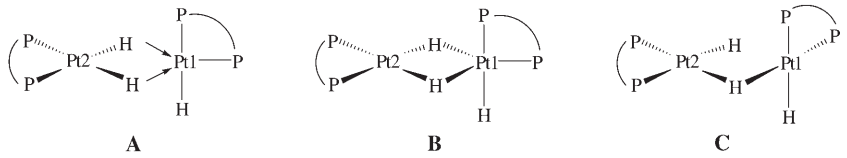

Scheme 3. Structural models contributing to the structure of complex **1**.

platinum centers, the respective coordination planes of which are almost perpendicular on the basis of the 83.4° angle that forms between the P1-Pt1-P2 and P3-Pt2-P4 planes (Figure 4). Notwithstanding this description, a high distortion is observed in the square-planar coordination geometry around Pt1 as, considering the mean plane formed by P1, P2, Pt1, H1, and H3 atoms, the maximum deviation from planarity is 0.47 Å.

None of the three models alone completely matches the observed structure, which, consequently, should be described as arising from the contribution of the three proposed structural types. However, DFT calculations performed in the **1t** model of **1** suggest that model **C** could be the most accurate way to describe complex **1**.

*Crystal Structure of [(dppp)Pt(μ-H)(μ-S)Pt(dppp)]ClO$_4$ (**2**)*: Crystals of **2** are cubic and consist of discrete [(dppp)Pt(μ-H)(μ-S)Pt(dppp)]$^+$ ions and disordered ClO_4^- counterions that fill the holes generated by the cations in the unit cell. Due to disorder problems these counterions were not been directly observed in the crystal structure. However, the presence of ClO_4^- ions in **2** is consistent with the reaction procedure and elemental analysis as well as with the intense broad band at 1100 cm^{-1} in the infrared spectrum. The overall geometry of the cation and the system used in labeling the principal atoms are shown in Figure 5. Selected bond distances and angles are presented in Table 5.

The dinuclear [(dppp)Pt(μ-H)(μ-S)Pt(dppp)]$^+$ ion has crystallographic C_2 symmetry, the rotation axis passing through the bridging sulfide and hydride ions. The latter could be directly located and successfully refined in the X-ray experiment. The main framework of this species can be described as being formed by a central {Pt(μ-H)(μ-S)Pt} core with an exactly planar, dihedral angle between the two PtHS planes $\theta = 180°$; the metal centers complete their coordination environment with chelating dppp ligands. As a result, two symmetry-related PtP_2C_3 rings with a distorted chair conformation are fused to the central core. The disposition of the two phosphorus atoms that belong to the same dppp ligand together with the bridging sulfide and hydride ions determine a slightly distorted square-planar configuration about each platinum atom, deviations from planarity being less than 0.04 Å. Other main structural features refer to the Pt–Pt distance of 2.825 Å, which is indicative of metal–metal interactions, and to the angle of 95.16° formed by the diphosphine ligand with the platinum atom, both values being consistent with data in the literature for related compounds.[20,31,32]

The structural parameters observed for [(dppp)Pt(μ-H)(μ-S)Pt(dppp)]$^+$ agree well with those reported for the closely related [(dppe)Pt(μ-H)(μ-S)Pt(dppe)]$^+$[32] and [(dppp)Pt(μ-S)$_2$Pt(dppp)][20] complexes. Comparison of the geometries of the {Pt(μ-H)(μ-S)Pt} core in the two former species shows that the nature of the terminal diphosphane ligand mainly affects the bond distances and angles that involve the bridging hydride ion. Therefore, the Pt–H bond distance is about 0.16 Å shorter and the Pt-H-Pt′ angle 14.7° greater in [(dppp)Pt(μ-H)(μ-S)Pt(dppp)]$^+$, this being concomitant with a slight lengthening in the Pt–Pt separation. Besides, while the {Pt(μ-H)(μ-S)Pt} core is strictly planar in **2**, the dihedral angle between the two PtHS planes is 177.6° for the dppe analogue.

Comparison between complexes [(dppp)Pt(μ-H)(μ-S)Pt(dppp)]$^+$ and [(dppp)Pt(μ-S)$_2$Pt(dppp)] also shows significant features. Therefore, the most remarkable effect accom-

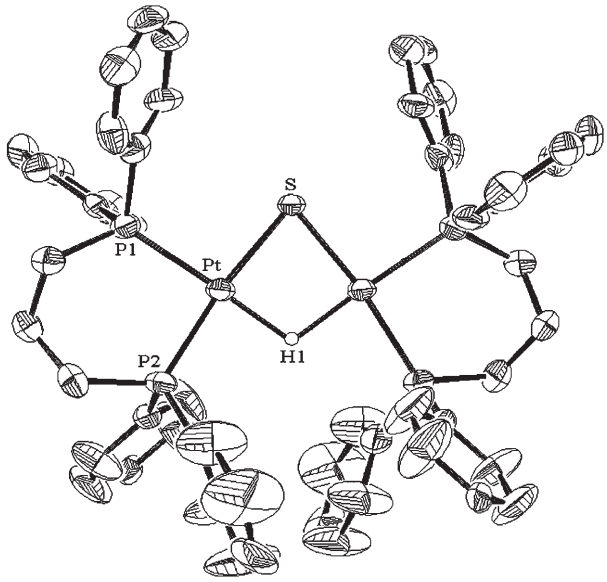

Figure 5. Structure of the cation in complex **2** with 50% probability displacement ellipsoids and selected atoms labels. H atoms are omitted, except for the bridging hydride.

Table 5. Selected bond lengths [Å] and angles [°] for complex **2**.

Pt–Pt′[a]	2.825(10)	Pt–P1	2.270(3)
Pt–S	2.288(3)	Pt–P2	2.280(3)
Pt–H1	1.74(10)	S···H1	2.837
Pt-S-Pt′[a]	76.23(12)	P1-Pt-Pt′[a]	144.00(8)
Pt-H1-Pt′[a]	107.44	P2-Pt-S	172.60(11)
P1-Pt-P2	95.16(13)	P2-Pt-H1	85(4)
P1-Pt-S	92.24(10)	P2-Pt-Pt′[a]	120.72(9)
P1-Pt-H1	176.7(18)	S-Pt-H1	88(4)

[a] Symmetry code: $^1/_2-x$, y, $^1/_2-z$.

panying the replacement of a bridging S by H in the {Pt(μ-X)(μ-S)Pt} core is that it is hinged for X=S (θ=134.8°) with a platinum–platinum distance of 3.235 Å, but exactly planar for X=H (θ=180°), for which this distance becomes 0.41 Å shorter. To make the planarity of the ring compatible with the shortening of the Pt–Pt distance, the Pt-S-Pt angle in **2** decreases up to 76.23°, compared with 87.52° in [(dppp)Pt(μ-S)$_2$Pt(dppp)]. However, the Pt–S bond length in **2**, 2.29 Å, is only slightly shorter than the average Pt–S distance in [(dppp)Pt(μ-S)$_2$Pt(dppp)], 2.34 Å. Analogously, the bite angle of the diphosphane ligand and the Pt–P distances are not significantly affected by the nature of X, S, or H in the mentioned core. The difference between the two Pt–P bond lengths in **2** (P *trans* to μ-S, 2.280 Å; P *trans* to μ-H 2.270 Å) is small but consistent with a *trans*-influence following the order: μ-S > μ-H. The ^1J(Pt,P) couplings found for **2** in solution, 2707 for Pt–P$_{trans\,to\,S}$ and 3752 Hz for Pt–P$_{trans\,to\,H}$ are also consistent with this ordering.

Theoretical study: Theoretical calculations have been performed in order to evaluate the feasibility of the processes described above. In calculations, the current dppp ligand has been modeled by $H_2P(CH_2)_3PH_2$ (dhpp). Calculated model species are labeled by adding a **t** to the number of the parent compound. In addition to determining the relative stabilities of the species proposed and thus obtaining the energetic picture of the aforementioned reactions, this study provides an insight into the structural features of the compounds involved. Some of the proposed intermediates have not been detected. Moreover, all the species bear hydrido ligands, and the intrinsic difficulty of using X-ray methods to accurately locate hydrogen atoms is well known. In contrast, quantum mechanical calculations have proven to be a cost-effective high-quality technique for precise location of hydride positions.[33] Overall, the theoretical study was made in order to contribute to the search for an answer to the following questions, which are difficult to address from an experimental point of view: 1) structure and fluxional behavior of [Pt$_2$(H)$_2$(μ-H)(dppp)$_2$]$^+$ (**1**); 2) structure of [Pt$_2$(H)$_2$(μ-SH)(dppp)$_2$]$^+$ (**Int 1**); 3) preferred protonation site in [Pt(H)(SH)(dppp)] (**3**); and 4) thermodynamic feasibility of the proposed pathways for the reaction from **3** to **2**.

Structure and fluxional behavior of [Pt$_2$(H)$_2$(μ-H)(dppp)$_2$]$^+$: Trihydride cations [Pt$_2$(H)$_3$(P∩P)$_2$]$^+$ have been widely investigated.[34] In solution they show fluxional behavior on the NMR timescale over a wide temperature range, and consequently only one resonance is observed for the hydrides in the ^{1}H NMR spectrum. However, in the solid state two distinct types of structures have been observed with either a {(H)Pt(μ-H)$_2$Pt} or a {(H)Pt(μ-H)Pt(H)} core, both depicted in Scheme 3, labeled **B** and **C**, respectively.

One terminal and two bridging hydride ligands have been found in the solid state structures of [Pt$_2$(H)$_3$(dppe)$_2$]$^+$[29] (neutron diffraction) and [Pt$_2$(H)$_3${(Ph$_2$PC$_5$H$_4$)$_2$Fe}$_2$]$^+$.[35] In contrast, the presence of one bridging and two terminal hydrides has been noted in the structures of [Pt$_2$(H)$_3$(dtbpp)$_2$]$^+$,[36] [Pt$_2$(H)$_3$(butaphos)$_2$]$^+$,[37] and [Pt$_2$(H)$_3$(dcype)$_2$]$^+$.[14] As described in this work, the X-ray diffraction of **1** made it possible to determine the structure of this complex, including the direct location of the hydrogen atoms. Overall, the structure of **1** is consistent with that reported in neutron diffraction studies for its dppe-containing analogue. Before commenting on the theoretical result, we should stress that factors such as the bite angle of the chelating ligands, the steric demand of the substituents on the phosphorous atoms and even more subtle factors such as crystal-packing forces could be responsible for the existence of different structures.[14] Calculations have been performed in a simplified model (dhpp instead of the actual dppp) in gas phase, which therefore does not consider the full subtlety of real systems. However, a joint analysis of the structural and energetic theoretical results and comparison with the experimental results can help to describe the bonding scheme on [Pt$_2$(H)$_3$(dppe)$_2$]$^+$. The calculated structure of **1t** is shown in Figure 6. Selected bond angles are given in Table 4 for comparison with the experimental values of **1**. Despite the simplifications, a relatively good agreement with the X-ray data is found in the optimized bond angles, suggesting that the model retains the main bonding features of **1**. Regarding the bond lengths in **1t**, one central hydride (H3) shows two Pt–H distances (1.799 and 1.711 Å) within the usual range for a Pt–H bridging bond, while the Pt–H distances for the other central hydride H2 (1.608 and 2.337 Å) are consistent with the existence of only one Pt–H bond. The presence of the three hydride ligands with different *trans* influence is reflected in the very different Pt–P bond lengths, ranging from 2.279 Å and 2.308 Å for the P *trans* to H3 to 2.387 and 2.416 Å for the P *trans* to H2 and H1, respectively. Nevertheless a significant discrepancy with the X-ray data is found on the Pt1–H2 distance (exptl: 2.07 Å, calcd: 2.337 Å).

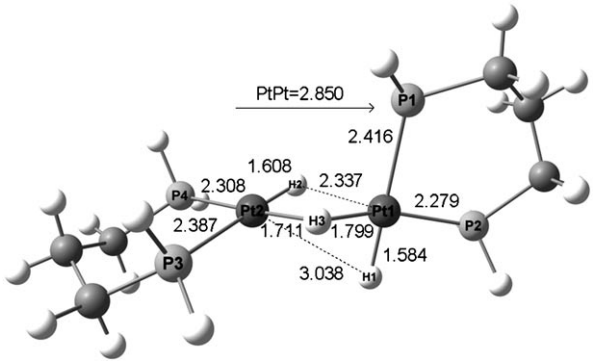

Figure 6. Optimized geometry of [Pt$_2$(H)$_2$(μ-H)(dhpp)$_2$]$^+$ (**1t**) with distances in Å.

Although, overall, the optimized geometry of **1t** seems to fit better with a type **C** structure (see Scheme 3), it remains unclear whether there is a bonding interaction between H2 and Pt1. This question has been theoretically analyzed from an energetic point of view. In our calculations we varied the Pt1···H2 distance between 2.05 and 2.65 Å by intervals of

0.1 Å. At each fixed value of this distance the remaining geometrical parameters were optimized. An extremely flat potential energy curve was eventually obtained, showing that Pt1–H2 stretching has a very low energy cost (less than 0.2 kcal mol^{-1}). These results support the non-existence of a bond between the Pt1 and H2 atoms and thus the presence of only one bridging hydride. The striking difference in the Pt1–H2 distance between the experimental and calculated structures can also be explained. With such a small energy change for Pt1–H2 stretching, this distance could be affected by crystal packing effects in the experimental system.

Inelastic neutron spectroscopy (INS) was used to investigate the vibrational modes of hydride ligands in $[Pt_2(H)_3(P\cap P)_2]^+$ complexes.[14] The different disposition of the H ligands around the Pt centers in structures **B** and **C** causes remarkable differences in the vibrational spectra. The stretching frequency for a terminal Pt–H group is expected to be in the region of 1900–2100 cm^{-1}, while the modes involving the μ-bridging H may be described in terms of symmetric and antisymmetric M-H-M stretching modes in the region of 1000–1400 cm^{-1}.[14] The calculated Pt–H frequencies fully agree with the ascription of a type **C** structure to **1t**. For the Pt–H stretching vibration that involves the non-bridging hydrides H1 and H2 two frequencies at 2119 cm^{-1} (Pt1–H1) and 1996 cm^{-1} (Pt2–H2) are obtained. The symmetric and anti-symmetric Pt-H3-Pt vibrational modes appear at 1240 and 1529 cm^{-1}, respectively.

Considering the X-ray structure of **1** and the set of calculations performed in the model complex **1t**, complex **1** can be considered to be formed by two square-planar {Pt(H)$_2$(dppp)} fragments that share the H3 hydride ligand. The dihedral angle between the planes defined by each metal center and its four ligands is about 90°, in agreement with the conformation detected in related cations.

Although the fast exchange of the hydride ligands in the $\{Pt_2H_3\}$ fragment, as shown by the equivalence of the three hydrides in the NMR spectra of $[Pt_2(H)_3(P\cap P)_2]^+$ complexes, is a well known phenomenon, the mechanism of the process remained unclear. Our computational study has shown that this phenomenon can be understood as a combination of the two dynamic processes depicted in Schemes 4 and 5.

The fluxional process depicted in Scheme 4 accounts for the equivalence of the bridging and non-bridging central hydrides H_a and H_b. A set of calculations decreasing the $Pt_b\cdots H_b$ distance from 2.05 Å to 1.75 Å and optimizing all the geometrical parameters at each fixed value of the $Pt_b\cdots H_b$ distance has been carried out. Taking the energy values at the $Pt_b\cdots H_b$ distance of 2.05, 1.95, 1.85, and 1.75 Å, the energy variation is negligible, less than 0.3 kcal mol^{-1}. It has been observed that the formation of the $Pt_b\cdots H_b$ bond is concomitant with the breaking of the $Pt_b\cdots H_a$ bond. Therefore, the dynamic process shown in Scheme 4 easily occurs with an almost inexistent energy barrier.

In addition to the above process (Scheme 4), the dynamic process shown in Scheme 5 is also a major contributor to the observed equivalence of all the hydride ligands of complex **1** in solution. This process consists of successive rotations along the Pt–H_a bonds. The thermodynamic feasibility of this process is confirmed by the low value (2.5 kcal mol^{-1}) of the energy difference between the two possible conformations (**1a** and **1b**, Scheme 5) of complex **1t**. The small increase in energy when going to structure **1b** in which no bonding interaction of H_b with Pt_b can be at work offers further proof of the very weak interaction between H_b and Pt_b in **1a**. The Pt–Pt bond is very weakly affected by the rotation. The Pt···Pt distance in **1b** is 2.932 Å, only 0.08 Å longer than in **1a**. The Pt–Pt interaction does not appear to be affected by this rotation, which contributes to the low energy cost of the process.

Structure of $[Pt_2(H)_2(\mu\text{-}SH)(dppp)_2]^+$: We have proposed that the formation of **2** by reaction of **1** with NaSH at 1:1 molar ratio takes place via an undetected intermediate complex, $[Pt_2(H)_2(\mu\text{-SH})(dppp)_2]^+$ (**Int1**). To make a structural proposal for this intermediate, DFT calculations were carried out considering that there are two possible arrangements for this species, one entailing a bridging SH group (**Int1$_{SH\text{-}b}$**) and the other a bridging hydride (**Int1$_{H\text{-}b}$**). The optimized structures are shown in Figure 7. The Pt–Pt distance varies notably by changing the bridging ligand, being much longer in the μ-SH (3.677 Å) than in the μ-H isomer (2.980 Å). The μ-SH isomer is notably more stable than the hydrido-bridged one, as **Int1$_{SH\text{-}b}$** lies 11.3 kcal mol^{-1} below **Int1$_{H\text{-}b}$**. Even if $[Pt_2(H)(\mu\text{-H})(SH)(dppp)_2]^+$ were initially formed by the substitution of a terminal hydride in **1** by the hydrogensulfide anion, it could easily convert into the more stable $[Pt_2(H)_2(\mu\text{-SH})(dppp)_2]^+$ form. As shown in Figure 7, the **Int1$_{SH\text{-}b}$** species displays a remarkable structural feature, probably relevant for its subsequent reactivity. The structure of **Int1$_{SH\text{-}b}$** can be described as two square-planar platinum units sharing a bridging SH ligand. The coordination planes of the two square-planar units are almost parallel. With this

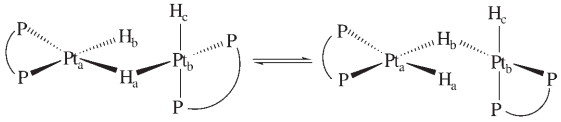

Scheme 4. Mechanism underlying the equivalence of the bridging hydride ligands.

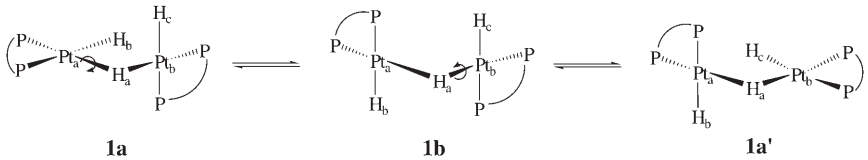

1a **1b** **1a'**

Scheme 5. Mechanism underlying the equivalence of the bridging and terminal hydride ligands.

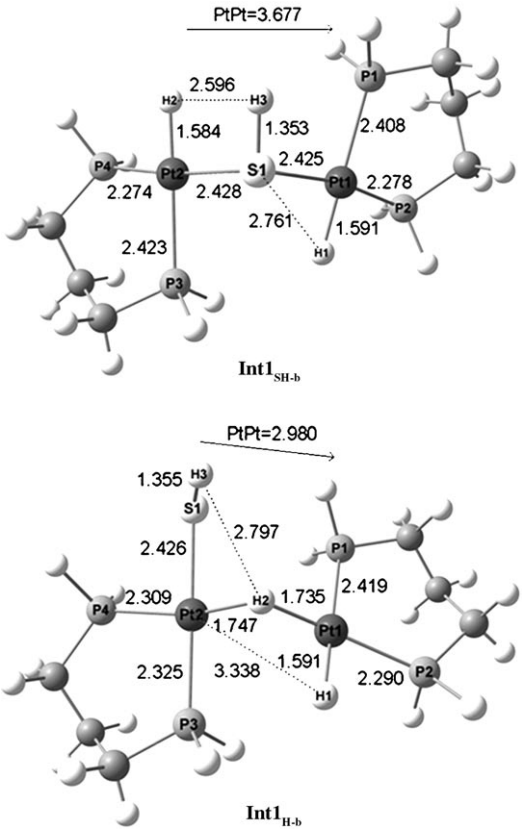

Figure 7. Optimized geometries for the μ-SH (**Int1$_{SH-b}$**) and μ-H isomers (**Int1$_{H-b}$**) of $[Pt_2(H)_2(SH)(dhpp)_2]^+$.

spatial arrangement the Pt–H and S–H bonds are aligned so that a four-sided ring defined by the Pt-H-H-S atoms is formed. This disposition places a proton and a hydride ion in close spatial vicinity, thus setting the system ready to give rise to the formation of H_2.

*Preferred protonation site in [Pt(H)(SH)(dppp)] (**3**)*: Our mechanistic proposal for the formation of **2** by addition of $HClO_4$ to **3** involves as a first step the protonation of the latter species, in which the SH and H ligands are potential protonation sites. Therefore, two isomers can be envisaged for the protonated intermediate **Int2**, depending on whether the SH (**Int2$_{SH-H}$**) or H (**Int2$_{H-H}$**) is protonated. The optimized structures are shown in Figure 8. The **Int2$_{SH-H}$** species is 19.4 kcal mol^{-1} more stable than **Int2$_{H-H}$**, providing evidence that the SH group is considerably more basic than the hydride ligand. Accordingly, it is reasonable to formulate **Int2** as $[Pt(H)(SH_2)(dppp)]^+$.

Comparison of the optimized structure of the protonated intermediates with that of the parent complex **3t** reveals two structural features of these two isomers. On the one hand, the H-protonated species has a dihydrogen ligand, as proved by the short H–H distance (0.787 Å). On the other, the protonation of the SH ligand causes considerable weakening of the Pt–S bond, as shown by the lengthening of the Pt–S distance from 2.381 Å in **3** to 2.457 Å in **Int2$_{SH-H}$**. Consistently, an easy SH_2 release from $[Pt(H)(SH_2)(dppp)]^+$ can be expected.

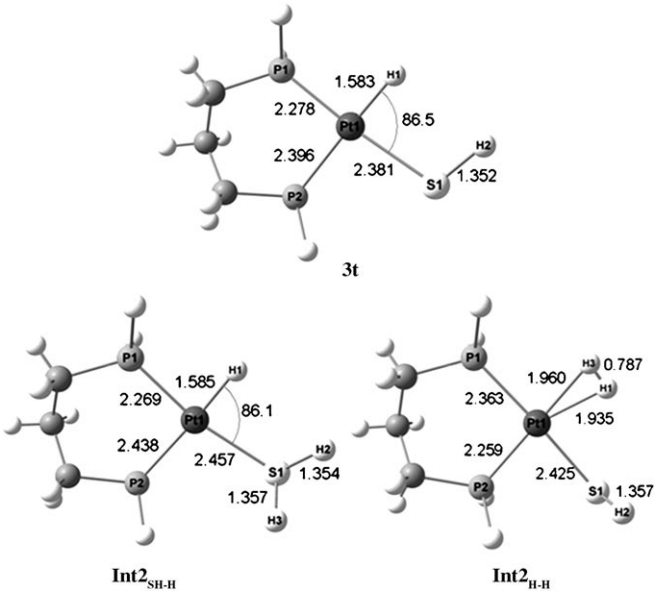

Figure 8. Optimized geometries of [Pt(H)(SH)(dhpp)] **3t** and corresponding S-protonated (**Int2$_{SH-H}$**) and H-protonated (**Int2$_{H-H}$**) derivatives.

*Thermodynamic feasibility of the proposed pathway for the reaction from **3** to **2***: DFT calculations were performed in order to discuss the thermodynamic feasibility of the pathway depicted in Scheme 1 for the formation of **2** from **3** in acidic medium. Calculated values of the reaction energies are collected in Table 6.

The proposed pathway for the reaction from **3** to **2** involves three steps. Following protonation of **3**, the second step involves the condensation of the protonated species $[Pt(H)(SH_2)(dppp)]^+$ with an additional molecule of **3**, which is accompanied by the release of SH_2 (reaction A in Table 6) and the formation of the $[Pt_2(H)_2(\mu\text{-}SH)(dppp)_2]^+$ intermediate (**Int1$_{SH-b}$**). This is a highly exothermic process ($\Delta E = -27.4$ kcal mol^{-1}). The third step (reaction B) is an intramolecular reaction in the **Int1$_{SH-b}$** species that consists of the formation of H_2 from a hydride ligand and the proton of the SH group. We have already commented that the spatial arrangement of the proton and the hydride in **Int1$_{SH-b}$** (Figure 7) should facilitate this reaction. The release of the

Table 6. Reaction energies [kcal mol^{-1}] for the **3**→**2** process.

	Reaction	ΔE
A	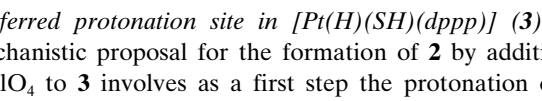	−27.4
B	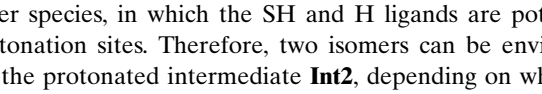	+6.5

H_2 molecule enables the remaining terminal hydride to shift to a bridging position and thus give rise to the {Pt(μ-S)(μ-H)Pt} core in **2** (Figure 9). Interestingly, the optimized structure of $[Pt_2(\mu\text{-H})(\mu\text{-S})(dhpp)_2]^+$ (**2t**) is fully consistent with the geometric parameters obtained from X-ray data. The Pt–P distances, although not very different, follow the same trend than those determined by X-ray (Pt–P *trans* to μ-S > Pt–P *trans* to μ-H) and are consistent with a *trans* influence following the trend μ-S > μ-H.

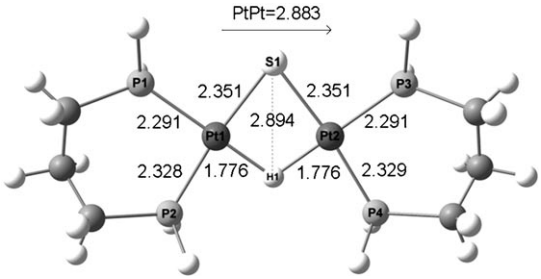

Figure 9. Optimized geometry of $[Pt_2(\mu\text{-H})(\mu\text{-S})(dhpp)_2]^+$.

The reversal of the reaction of H_2 formation from S–H and Pt–H is the heterolytic splitting of H–H bond by means of a transition-metal bonded to an S ligand. This reaction is well documented in the literature.[38] Reaction B is slightly endothermic (+6.5 kcal mol^{-1}). However, this value is largely compensated by the exothermicity of reaction A. Overall, the proposed pathway from **3** to **2** through intermediate $\mathbf{Int1_{SH\text{-}b}}$ is highly favored on thermodynamic grounds (ΔE = −20.9 kcal mol^{-1}).

We have also invoked the role of the intermediate $\mathbf{Int1_{SH\text{-}b}}$ in the conversion of **1** to **2** by reaction of the former with NaSH. Once $\mathbf{Int1_{SH\text{-}b}}$ is formed, the release of H_2 leads to **2**, as already proposed as the third step in the reaction from **3** to **2** (reaction B in Table 6). Although this process is slightly endothermic, it could be favored by the liberation of H_2.

Conclusions

The set of reactions investigated in this work provides solid evidence that behind the apparent simplicity of platinum complexes containing Pt–H, Pt–SH, or Pt–S fragments, they have an outstanding chemistry. This can be attributed to a combination of several factors that are put to work at the same time. A perspective view of the reactions depicted in Scheme 1 indicates that the strong tendency of sulfide and hydrogensulfide ligands to bind to platinum, the ability of the sulfide ion to bridge two platinum centers, and the amphoteric behavior of the hydrogen sulfide group in the Pt–SH fragment are key aspects of the observed reactivity. Furthermore, the ability of the hydride ligand in the Pt–H fragment to act as a base capable of forming H_2 by reaction with the proton of the SH group accounts for the conversion: from **1** to **2** and from **2** to **4**, by addition of NaSH; from **3** to **2** by addition of $HClO_4$; and from **3** to **4** by addition of [Pt(dppp)(SH)$_2$]. Interestingly, while the conversion of the {Pt(μ-H)(μ-S)Pt} core in **2** into {Pt(μ-S)$_2$Pt} in **4** is easily achieved by addition of excess NaSH, the reverse reaction, which implies the replacement of a sulfide with a hydride ligand, requires previous formation of **5**, an unprecedented dinuclear complex containing a Pt–Pt bonded $\{Pt_2^{I}(\mu\text{-S})\}$ core, which was unreported.

Our previous studies of the chemistry of $[Pt_2(\mu\text{-S})_2(P\cap P)_2]$ complexes showed the exceptional ability of the $\{Pt_2S_2\}$ core to react with virtually any electron-acceptor species.[13] The reactions described here extend the richness of this chemistry. They also show that the formation and further evolution of platinum complexes containing Pt–H, Pt–SH, or Pt–S fragments is highly dependent on the reaction conditions such as acid–base properties and solution temperature, and thus, prediction of their exact nature in solution should not be considered obvious. Within the context of this reactivity, the reported findings may be relevant in the study of platinum-mediated homogeneous hydrodesulfurization processes. Research in this direction is being pursued by our group.

Experimental Section

Materials and methods: All reactions were carried out at room temperature under an atmosphere of pure dinitrogen, and conventionally dried and degassed solvents were used throughout. These were Purex Analytical Grade from SDS. Metal complexes of formula [PtCl$_2$(dppp)] and [Pt(SH)$_2$(dppp)] were prepared in accordance with published methods.[39,12b] Complexes [Pt(H)(SH)(dppp)] (**3**), $[Pt_2(H)_3(dppp)_2]^+$, and [(dppp)Pt(μ-S)$_2$Pt(dppp)] (**4**) were obtained by alternative procedures.[16b,15,20] Commercial Na_2S, $Na_2S{\cdot}9H_2O$, $NaBH_4$, and $NaBD_4$ compounds were used without further purification. NaSH was obtained from commercial $NaSH{\cdot}xH_2O$ by keeping it under vacuum overnight. Elemental Analyses were performed on a Carlo-Erba CHNS EA-1108 analyzer. IR spectra were recorded on a Perkin–Elmer FT-2000 spectrophotometer using KBr pellets (s = strong, m = medium, br = broad band). ^{1}H, ^{1}H{^{31}P}, ^{31}P, ^{31}P{^{1}H} ^{195}Pt, and ^{195}Pt{^{1}H} NMR spectra as well as the ^{195}Pt,^{1}H and ^{31}P,^{1}H HMBC (heteronuclear multiple-bond correlation) and ^{1}H,^{1}H NOE (nuclear Overhauser effect) experiments were performed from samples in $(CD_3)_2SO$ or $CDCl_3$ at room temperature, unless otherwise indicated, with a Bruker Avance DRX-360 spectrometer operating at 360.13 MHz for ^{1}H, 145.79 MHz for ^{31}P and 77.42 MHz for ^{195}Pt. ^{1}H chemical shifts are relative to $SiMe_4$, ^{31}P chemical shifts to external 85% H_3PO_4 and ^{195}Pt chemical shifts are relative to external 1 M $Na_2[PtCl_6]$ in D_2O. ^{2}H NMR experiments were performed from samples in $CDCl_3/CHCl_3$ mixtures at room temperature with a Bruker Avance 500 operating at 76.75 MHz. ^{2}H NMR chemical shifts are relative to $CDCl_3$. ^{31}P{^{1}H} NMR spectra were simulated on a Pentium-200 computer using the gNMR V4.0.1 program.[40] The ESI-MS measurements were performed on a VG Quattro Micromass Instrument. Experimental conditions were as follows: 10 μL of sample was injected at 15 μL min^{-1}; capillary-counter electrode voltage, 4.5 kV; lens-counter electrode voltage 1.0 kV; cone potential, 55 V; source temperature, 90 °C; *m*/*z* range, 300–1600. The carrier was a 1:1 mixture of acetonitrile and water containing formic acid (1–20%). ESI-MS and NMR data for complexes **1**–**5** synthesized in this work are given in Table 1.

Evolution of complexes **1**–**5** under various experimental conditions as well as the optimal conditions for their synthesis was obtained by monitoring the corresponding reactions by means of ^{1}H and ^{31}P NMR spectroscopy. These results are summarized in Table 2. The general procedure consisted of adding controlled amounts of the reagent to a solution of

the corresponding pure compound (50 mg) in solvent (10 mL). At different times, usually every 20 min, aliquots were taken from the mother solution, and were evaporated to dryness, and the ^{1}H and ^{31}P NMR spectra in [D$_6$]DMSO or $CDCl_3$ were recorded. These showed that, except for the reaction of **2** with excess NaSH that leads to an equimolar mixture of two platinum complexes, the disappearance of the starting platinum complex is concomitant with the formation of a new platinum species, which does not undergo further conversion. However, the reaction times involved for a maximum yield vary, ranging from 1 to 12 h. On the basis of all these data, the synthetic procedures selected are described below.

Caution: *Although no problem has been encountered in this work, all perchlorate compounds are potentially explosive, and should be handled in small quantities and with great care!*

Synthesis of [(dppp)Pt(H)$_2$(μ-H)Pt(dppp)]ClO$_4$ (1): Solid [PtCl$_2$(dppp)] (500 mg, 0.74 mmol) was added to a solution of $NaBH_4$ (56 mg, 1.48 mmol) in absolute ethanol (100 mL) and the mixture was stirred at room temperature for 4 h. Addition of $NaClO_4$ (45 mg, 0.37 mmol) caused precipitation of an off-white solid. This was collected by filtration, washed with ethanol and diethyl ether, and vacuum dried. Yield 85 %; elemental analysis calcd (%) for $C_{54}H_{55}ClO_4P_4Pt_2$: C 49.23, H 4.21; found: C 49.12, H 4.13; IR: $\tilde{\nu}$ = 2033 (m; Pt–H); 1094 cm^{-1} (s, br; ClO_4). Diffusion of diethyl ether into a solution of the solid complex in acetonitrile afforded colorless crystals suitable for X-ray diffraction.

The deuterated analogue **1d** was obtained by the same procedure with [PtCl$_2$(dppp)] and $NaBD_4$ at a 1:4 molar ratio. On the one hand, the ^{2}H NMR spectrum of **1d** is fully consistent with the deuteration of the {Pt$_2$H$_3$} core: ^{2}H NMR ($CDCl_3$ + $CHCl_3$) δ = −3.65 ppm (t ^2J(D,P) < 10 Hz, ^1J(H,Pt) = 71 Hz). On the other, the ^{1}H NMR spectrum in the high-field region gives evidence of the presence of {PtD$_2$HPt} (δ = −3.62 ppm (qq, ^2J(H,P) = 40.2 Hz, ^1J(H,Pt) = 460.6 Hz), {PtDH$_2$Pt} (δ = −3.65 ppm (qq, ^2J(H,P) = 39.9 Hz, ^1J(H,Pt) = 459.0 Hz) and {PtH$_3$Pt} (δ, ^2J(H,P) and ^1J(H,Pt) values are given in Table 1). These results and ESI-MS data show that complex **1d** is an isotopic mixture of the trideuteride, hydridodideuteride, dihydridodeuteride, and trihydrido complexes. The three former species are in 75:15:10 molar ratios, while there is a negligible amount of the latter (< 1 %). The relative amounts are deduced from the integration of the signals of the hydrido ligands with respect to the protons of the aliphatic CH_2 groups in the phosphane ligands. The presence of all different isotopomers in the cation of **1d** has already been reported.[41]

Synthesis of [(dppp)Pt(μ-H)(μ-S)Pt(dppp)]ClO$_4$ (2): Complex **1** (200 mg, 0.15 mmol) was added to a solution of $Na_2S{\cdot}9H_2O$ (88 mg, 0.36 mmol) in benzene (50 mL) and the mixture was stirred at room temperature for 6 h. The excess $Na_2S{\cdot}9H_2O$ was filtered off. Concentration of the resulting solution to about 5 mL and addition of diethyl ether yielded a yellow-orange solid. This was washed with diethyl ether and vacuum dried. Yield 85 %; elemental analysis calcd (%) for $C_{54}H_{53}ClO_4P_4Pt_2S$: C 48.13, H 3.96, S 2.38; found: C 48.01, H 3.82, S 2.49; IR: ν = 1094 cm^{-1} (s, br; ClO_4). Recrystallization of this compound in benzene gave yellow crystals suitable for X-ray diffraction.

The deuterated analogue **2d** was obtained in about 75 % yield by replacing **1** with **1d** in the above procedure with Na_2S at a 1:2 molar ratio. On the basis of ^{1}H and ^{2}H NMR data, **2d** consists of a mixture of the {Pt(μ-D)(μ-S)} and {Pt(μ-H)(μ-S)} cores at an approximate 86:14 molar ratio. ^{2}H NMR ($CDCl_3$ + $CHCl_3$) δ = −5.17 ppm (t, ^2J(D,P(*cis*)) < 5 Hz; ^2J(D,P(*trans*)) = 10.5 Hz; with satellites, ^1J(D,Pt) = 43.1 Hz).

Synthesis of [Pt(H)(SH)(dppp)] (3): Complex **1** (200 mg, 0.15 mmol) was added to a solution of NaSH (126 mg, 2.25 mmol) in benzene (50 mL) and the mixture was stirred at room temperature for 3 h. The remaining solid residue was filtered off and the solution was concentrated to about 5 mL. Addition of diethyl ether yielded a yellow solid. This was washed with diethyl ether and vacuum dried. Yield 75 %; elemental analysis calcd (%) for $C_{27}H_{28}P_2PtS$: C 50.54, H 4.40, S 5.00; found: C 50.49, H 4.36, S 5.12.

The deuterated analogue **3d** was obtained in about 71 % yield by replacing **1** with **1d** in the above procedure. On the basis of ^{1}H and ^{2}H NMR data **3d** consists of a mixture of the two {Pt(D)(SH)} and {Pt(H)(SH)} fragments at an approximate 82:18 molar ratio. ^{2}H NMR ($CDCl_3$ + $CHCl_3$, δ): −3.93 ppm (td, ^2J(D,P(*cis*)) < 5 Hz; ^2J(D,P(*trans*)) = 29.5 Hz; ^1J(D,Pt) = 145 Hz).

Synthesis of [(dppp)Pt(μ-S)Pt(dppp)] (5): Complex **4** (200 mg, 0.16 mmol) was added to an solution of $NaBH_4$ (24 mg, 0.64 mmol) in absolute ethanol (50 mL) and the mixture was stirred at room temperature for 6 h. The resultant solution was filtered through Celite and the filtrate evaporated to dryness. The solid residue was extracted with a few milliliters of benzene. The crude product was precipitated from the benzene solution by addition of diethyl ether. The yellow solid thus obtained was collected by filtration, washed with diethyl ether and vacuum dried. Yield 85 %; elemental analysis calcd (%) for $C_{54}H_{52}P_4Pt_2S$: C 52.00, H 4.20, S 2.57; found: C 51.92, H 4.22, S 2.60. Attempts to obtain crystals suitable for X-ray diffraction were unsuccessful.

X-ray crystallographic characterization: A summary of crystal data, data collection, and refinement parameters for the structural analysis of complexes **1** and **2** is given in Table 7. Measurements of diffraction intensity data were collected on a Bruker SMART CCD-1000 area-detector diffractometer with graphite-monochromated $Mo_{K\alpha}$ radiation (λ = 0.71073 Å). Absorption correction was carried out by semiempirical methods based on redundant and symmetry-equivalent reflections with the aid of the SADABS program.[42] Cell parameters were obtained from a least-squares fit on the observed setting angles of all significant intensity reflections. The structures were resolved by direct methods and refined by full-matrix least-squares based on F^2, with the aid of SHELX-97 software.[43] All non-hydrogen atoms were anisotropically refined. Hydrogen atoms, except for hydride ligands, were included at geometrically calculated positions with thermal parameters derived from the parent atoms. In compound **2** the solvent and anion molecules appear to be highly disordered thus making it difficult to model its position and distribution reliably. Therefore, the SQUEEZE function was used to eliminate the contribution of the electron density in the disordered solvent region from the measured intensity data and therefore the solvent-free data was employed in the final refinement. The contribution of the disordered anions to the diffraction pattern was incorporated in the model using PLATON/SQUEEZE.[44] A total of 1178 e$^-$ were found in several voids with a total volume of 3003 Å^3. The total amount of charge approximately accounts for the remaining 24 ClO_4^- ions disordered in the unit cell (24 × 50 e$^-$ =

Table 7. Crystallographic data for complexes **1** and **2**.

	1·0.5($C_4H_{10}O$)	**2**
formula	$C_{54}H_{55}ClO_4P_4Pt_2{\cdot}0.5\,C_4H_{10}O$	$C_{54}H_{53}ClO_4P_4Pt_2S$[a]
M_r	1354.6	1347.5
crystal system	monoclinic	cubic
space group	$P2_1/n$	$I\bar{4}3d$
a [Å]	17.1193(8)	31.1962(16)
b [Å]	17.9197(9)	31.1962(16)
c [Å]	17.1544(8)	31.1962(16)
α [°]	90	90
β [°]	102.027(2)	90
γ [°]	90	90
V [Å^3]	5147.0(4)	30360(2)
T [K]	100.0(1)	120(1)
Z	4	24
ρ_{calcd} [g cm^{-3}]	1.742	1.638
μ [mm^{-1}]	5.653	5.725
reflns collected	31887	78467
unique reflns (R_{int})	26229 (0.0703)	4326 (0.084)
parameters/restraints	818/0	277/72
goodness-of-fit on F^2	1.079	1.094
$R1$, $wR2$ [$I > 2\sigma(I)$]	0.0244, 0.0512	0.0437, 0.0994
$R1$, $wR2$ (all data)	0.0386, 0.057	0.0635, 0.1118
largest diff. peak/hole [e Å^{-3}]	1.38/−1.387	0.652/−0.859

[a] The ClO_4^- ions show disorder (see text).

1200 e^-) needed to counterbalance the positive charge of the complex. Molecular graphics are represented by Ortep-3 for Windows.

CCDC-606465 (**1**) and CCDC-606466 (**2**) contains the supplementary crystallographic data for this paper. These data can be obtained free of charge from The Cambridge Crystallographic Data Centre via www.ccdc.cam.ac.uk/data_request/cif.

Computational details: Calculations were performed with the GAUSSIAN 98 series of programs.[45] Density functional theory (DFT) was applied with the B3LYP functional.[46] Effective core potentials (ECP) were used to represent the innermost electrons of the platinum atom as well as the electron core of P and S atoms.[47] The basis set for Pt was that associated with the pseudopotential, with a standard double-ζ LANL2DZ contraction.[45] The basis set for the P and S atoms was that associated with the pseudopotential, with a standard double-ζ LANL2DZ contraction[45] supplemented with a set of d-polarization functions.[48] A 6–31G basis set was used for C and the H bound to P or C atoms.[49] For H atoms bound to the Pt and S atoms or in H_2 molecule, a 6–31G(d,p) basis set was used.[50]

Acknowledgements

This research was supported by the Ministerio de Educación y Ciencia, (MEC, Spain, Grants CTQ2004–01463, and CTQ2005–09000-C02–01). FNV is indebted to MEC for a pre-doctoral scholarship. We are grateful to Dr. T. Parella and Dr. J. Sola of the UAB for interesting discussions on NMR data, and to Dr. A. L. Llamas and Dr. B. Dacuña of the USC for crystal structure determination.

[1] A search in the Scifinder Scholar V.2006 database with hydrodesulfurization/petroleum as the entry yields more than 4000 articles, about 1000 in the decade 1980–90 and, since then, about 2000.
[2] a) US Environmental Protection Agency (http://www.epa.gov/otaq/gasoline.htm); b) European Union, EU Directive 93/12/EEC, 1993 and Amending acts (98/70/EEC, 99/32/EEC, 05/33/EEC).
[3] a) H. Topsøe, B. S. Clausen, F. E. Massoth, *Hydrotreating Catalysis, Science and Technology, Vol. 11* Springer, Berlin, **1996**; b) R. R. Chianelli, M. Daage, M. J. Ledoux, *Adv. Catal.* **1994**, *40*, 177–234.
[4] a) R. J. Angelici, *Acc. Chem. Res.* **1988**, *21*, 387–394; b) R. J. Angelici, *Polyhedron* **1997**, *16*, 3073–3088; c) W. D. Jones, D. A. Vicic, R. M. Chin, J. H. Roache, A. W. Myersd, *Polyhedron* **1997**, *16*, 3115–3128.
[5] R. J. Angelici, *Organometallics* **2001**, *20*, 1259–1275 and references therein.
[6] A. Iretskii, H. Adams, J. J. García, G. Picazo, P. M. Maitlis, *Chem. Commun.* **1998**, 61–62.
[7] a) J. J. García, B. E. Mann, H. Adams, N. A. Bailey, P. M. Maitlis, *J. Am. Chem. Soc.* **1995**, *117*, 2179–2186; b) J. J. García, P. M. Maitlis, *J. Am. Chem. Soc.* **1993**, *115*, 12200–12201; c) J. J. García, A. Arévalo, S. Capella, A. Chehata, M. Hernández, V. Montiel, G. Picazo, F. Del Río, R. Toscano, H. Adams, P. M. Maitlis, *Polyhedron* **1997**, *16*, 3185–3195; d) D. A. Vicic, W. D. Jones, *Organometallics* **1998**, *17*, 3411–3413.
[8] J. J. García, A. Arévalo, V. Montiel, F. Del Río, B. Quiroz, H. Adams, P. M. Maitlis, *Organometallics* **1997**, *16*, 3216.
[9] H. Li, G. B. Carpenter, D. A. Sweigart, *Organometallics* **2000**, *19*, 1823–1825.
[10] M. Capdevila, P. González-Duarte, I. Mira, J. Sola, W. Clegg, *Polyhedron* **1992**, *11*, 3091–3093.
[11] D. A. Vicic, W. D. Jones, *J. Am. Chem. Soc.* **1999**, *121*, 7606–7617.
[12] a) G. Aullón, M. Capdevila, W. Clegg, P. González-Duarte, A. Lledós, R. Mas-Ballesté, *Angew. Chem.* **2002**, *114*, 2900–2902; *Angew. Chem. Int. Ed.* **2002**, *41*, 2776–2778; b) R. Mas-Ballesté, G. Aullón, P. A. Champkin, W. Clegg, C. Mégret, P. González-Duarte, A. Lledós, *Chem. Eur. J.* **2003**, *9*, 5023–5035.
[13] P. González-Duarte, A. Lledós, R. Mas-Ballesté, *Eur. J. Inorg. Chem.* **2004**, *18*, 3585–3599.
[14] A. L. Bandini, G. Banditelli, M. Manassero, A. Albinati, D. Colognesi, J. Eckert, *Eur. J. Inorg. Chem.* **2003**, 3958–3967.
[15] C. B. Knobler, H. D. Kaesz, G. Minghetti, A. L. Bandini, G. Banditelli, F. Bonati, *Inorg. Chem.* **1983**, *22*, 2324–2331.
[16] a) R. Ugo, G. La Monica, S. Cenini, A. Segre, F. Conti, *J. Chem. Soc. A* **1971**, 522–528; b) F. Cecconi, P. Innocenti, S. Midollini, S. Moneti, A. Vacca, J. A. Ramirez, *J. Chem. Soc. Dalton Trans.* **1991**, 1129–1134.
[17] T. Miyamoto, *J. Organomet. Chem.* **1977**, *134*, 335–362.
[18] B. S. Haggerty, C. E. Housecroft, A. L. Rheingold, B. A. M. Shaykh, *J. Chem. Soc. Dalton Trans.* **1991**, 2175–2184.
[19] I. M. Blacklaws, E. A. V. Ebsworth, D. W. H. Rankin, H. E. Robertson, *J. Chem. Soc. Dalton Trans.* **1978**, 753–758.
[20] R. Mas-Ballesté, M. Capdevila, P. A. Champkin, W. Clegg, R. A. Coxall, A. Lledós, C. Mégret, P. González-Duarte, *Inorg. Chem.* **2002**, *41*, 3218–3229.
[21] A. Shaver, M. El-khateeb, A. M. Lebuis, *Angew. Chem.* **1996**, *108*, 2510–2512; *Angew. Chem. Int. Ed. Engl.* **1996**, *35*, 2362–2363.
[22] C. H. Chin, T. S. A. Hor, *J. Organomet. Chem.* **1996**, *509*, 101–104.
[23] D. G. Evans, M. F. Hallam, D. M. P. Mingos, W. M. Wardle, *J. Chem. Soc. Dalton Trans.* **1987**, 1889–1895.
[24] H. Liu, A. L. Tan, K. F. Mok, T. C. W. Mak, A. S. Batsanov, J. A. K. Howard, T. S. A. Hor, *J. Am. Chem. Soc.* **1997**, *119*, 11006–11011.
[25] G. B. Robertson, W. A. Wickramasinghe, *Acta Crystallogr. Sect. C* **1987**, *43*, 1694–1697.
[26] A. L. Bandini, G. Banditelli, M. Grassi, A. Ponti, *Dalton Trans.* **2004**, 2027–2035.
[27] a) N. Hadj-Bagheri, R. J. Puddephatt, *Inorg. Chem.* **1989**, *28*, 2384–2388; b) H. Liu, A. L. Tan, K. F. Mok, T. S. A. Hor, *J. Chem. Soc. Dalton Trans.* **1996**, 4023–4026; c) C. T. Hunt, G. T. Matson, A. L. Balch, *Inorg. Chem.* **1981**, *20*, 2270–2276.
[28] M. Capdevila, W. Clegg, P. Gonzalez-Duarte, B. Harris, I. Mira, J. Sola, I. C. Taylor, *J. Chem. Soc. Dalton Trans.* **1992**, *19*, 2817–2826.
[29] M. Y. Chiang, R. Bau, G. Minghetti, A. L. Bandini, G. Banditelli, T. F. Koetzle, *Inorg. Chem.* **1984**, *23*, 122–124.
[30] A. W. Addison, N. Rao, J. Reedijk, J. van Rijn, G. C. Verschoor, *J. Chem. Soc. Dalton Trans.* **1984**, 1349–1356.
[31] a) G. Minghetti, A. L. Bandini, G. Banditelli, F. Bonati, R. Szostak, C. E. Strouse, C. B. Knobler, H. D. Kaesz, *Inorg. Chem.* **1983**, *22*, 2332–2338; b) A. L. Bandini, G. Banditelli, M. A. Cinellu, G. Sanna, G. Minghetti, F. Demartin, M. Manassero, *Inorg. Chem.* **1989**, *28*, 404–410; c) G. Minghetti, A. Albinati, A. L. Bandini, G. Banditelli, *Angew. Chem.* **1985**, *97*, 119–120; *Angew. Chem. Int. Ed. Engl.* **1985**, *24*, 120–121.
[32] W. Clegg, M. Capdevila, P. González-Duarte, J. Sola, *Acta Crystallogr. Sect. B* **1996**, *52*, 270–276.
[33] F. Maseras, A. Lledós, E. Clot, O. Eisesenstein, *Chem. Rev.* **2000**, *100*, 601–636.
[34] V. K. Jain, L. Jain, *Coord. Chem. Rev.* **2005**, *249*, 3075–3197, and references therein.
[35] B. S. Haggerty, C. E. Housecroft, A. L. Rheingold, B. A. M. Shaykh, *J. Chem. Soc. Dalton Trans.* **1991**, *8*, 2175–2184.
[36] T. H. Tulip, T. Yamagata, T. Yoshida, R. D. Wilson, J. A. Ibers, S. Otsuka, *Inorg. Chem.* **1979**, *18*, 2239–2250.
[37] A. L. Bandini, G. Banditelli, E. Cesarotti, F. Demartin, M. Manassero, G. Minghetti, *Gazz. Chim. Ital.* **1994**, *124*, 43–50.
[38] a) G. J. Kubas, *Adv. Inorg. Chem.* **2004**, *56*, 127–177; b) A. Ienco, M. J. Calhorda, J. Reinhold, F. Reineri, C. Bianchini, M. Peruzzini, F. Vizza, C. Mealli, *J. Am. Chem. Soc.* **2004**, *126*, 11954–11965.
[39] M. P. Brown, R. J. Puddephatt, M. Rashidi, K. R. Seddon, *J. Chem. Soc. Dalton Trans.* **1977**, 951–955.
[40] P. H. M. Budzelaar, *gNMR V4.01*, Cherwell Scientific, Oxford (UK), **1997**.
[41] G. Banditelli, A. L. Bandini, *Organometallics* **2006**, *25*, 1578–1582.
[42] *Area-Detector Absortion Correction*, Siemens industrial Automation, Madison, WI, **1996**.

[43] G. M. Sheldrick, SHELX-97 (SHELXS 97 and SHELXL 97), Program for the solution of Crystal Structures, University of Göttingen, Göttingen (Germany), **1998**.
[44] P. van der Sluis, A. L. Spek, *Acta Crystallogr. Sect. A* **1990**, *46*, 194–201; A. L. Spek, *J. Appl. Crystallogr.* **2003**, *36*, 7–13.
[45] Gaussian 98 (Revision A.9), M. J. Frisch, G. W. Trucks, H. B. Schlegel, G. E. Scuseria, M. A. Robb, J. R. Cheeseman, V. G. Zakrzewski, J. A. Montgomery, R. E. Stratmann, J. C. Burant, S. Dapprich, J. M. Millam, A. D. Daniels, K. N. Kudin, M. C. Strain, O. Farkas, J. Tomasi, V. Barone, M. Cossi, R. Cammi, B. Mennucci, C. Pomelli, C. Adamo, S. Clifford, J. Ochterski, G. A. Petersson, P. Y. Ayala, Q. Cui, K. Morokuma, D. K. Malick, A. D. Rabuck, K. Raghavachari, J. B. Foresman, J. Cioslowski, J. V. Ortiz, B. B. Stefanov, G. Liu, A. Liashenko, P. Piskorz, I. Komaromi, R. Gomperts, R. L. Martin, D. J. Fox, T. Keith, M. A. Al-Laham, C. Y. Peng, A. Nanayakkara, C. Gonzalez, M. Challacombe, P. M. W. Gill, B. G. Johnson, W. Chen, M. W. Wong, J. L. Andres, M. Head-Gordon, E. S. Replogle, J. A. Pople, Gaussian, Inc., Pittsburgh, PA, **1998**..
[46] a) C. T. Lee, W. T. Yang, R. G. Parr, *Phys. Rev. B* **1988**, *37*, 785–789; b) A. D. Becke, *J. Chem. Phys.* **1993**, *98*, 5648–5652; c) P. Stephens, F. Devlin, C. Chabalowski, M. Frisch, *J. Phys. Chem.* **1994**, *98*, 11623–11627.
[47] a) W. R. Wadt, P. J. Hay, *J. Chem. Phys.* **1985**, *82*, 284–298; b) P. J. Hay, W. R. Wadt, *J. Chem. Phys.* **1985**, *82*, 299–310.
[48] A. Höllwarth, M. Bohme, S. Dapprich, A. Ehlers, A. Gobbi, V. Jonas, K. Kohler, R. Stegmann, A. Veldkamp, G. Frenking, *Chem. Phys. Lett.* **1993**, *208*, 237–240.
[49] W. Hehre, R. Ditchfie, J. Pople, *J. Chem. Phys.* **1972**, *56*, 2257–2261.
[50] P. Harihara, J. Pople, *Theor. Chim. Acta* **1973**, *28*, 213–222.

Received: May 17, 2006
Revised: October 18, 2006
Published online: December 19, 2006

